Present-day neutron diffraction at pulsed neutron sources

A. M. Balagurov
Joint Institute for Nuclear Research, Dubna

Fiz. Elem. Chastits At. Yadra **23**, 1088–1143 (July–August 1992)

The current status of neutron-diffraction experiments at pulsed neutron sources is described. The general problems in time-of-flight neutron-diffraction studies are discussed. High-resolution experiments on polycrystalline materials, structure analysis, and special experiments using single crystals are discussed, along with studies of transient processes of short duration. Special attention is paid to recent topics: very high-resolution diffractometry, neutron Fourier diffractometers, and real-time studies.

INTRODUCTION

Neutron diffractometers have long been essential tools at research nuclear reactors. The number of experiments carried out using them and the amount of information acquired are so large they can hardly be estimated. The data obtained using neutron diffraction is of indisputable importance. It can therefore be stated that neutron diffraction has been fully accepted as one of the basic techniques for studying condensed media at the microscopic scale.

A characteristic feature of the current status of neutron diffraction is its continuing rapid development. This is mainly due to overall technical progress: the increased power of sources, the appearance of a new generation of electronics, the development of neutron detection methods, in particular, the appearance of position-sensitive detectors, and so on. It is important that improvement of the quantitative features of diffraction experiments has made it possible to undertake qualitatively new studies, which in principle could not be done before. However, perhaps the most important step in the development of neutron diffraction has been the creation of powerful pulsed neutron sources.

Already in the late 1960s, Brugger predicted[1] that it would be pulsed sources that would replace the generation of high-flux stationary research reactors constructed at that time. It is now clear that this prediction was true in the sense that in the 1970s and early 1980s an entire series of powerful pulsed neutron sources were actually constructed: the IBR-30 at JINR in 1970, the WNR (LANSCE since 1986) in the United States in 1977, the IPNS-1 in the United States in 1981, the IBR-2 at JINR in 1984, and the SNS in England and KENS-1 in Japan in 1985.

In recent years time-of-flight neutron diffractometers have been constructed at these sources. Not only do they offer possibilities comparable to those of ordinary diffractometers at stationary reactors, but in many characteristics they are better. The techniques developed for performing experiments at the new diffractometers are also not inferior to the traditional ones. The output of the new diffractometers is quite high and, in spite of the fact that they are still few in number, the studies carried out using them are becoming more and more important in the area of neutron-diffraction studies.

Here we shall review the status of neutron-diffraction studies at pulsed sources at the beginning of the 1990s. Our review has a methodological focus, i.e., most of the attention is given to methods of extracting and analyzing crystallographic and crystallophysical information from the data obtained in diffraction experiments at pulsed neutron sources and to comparison of the possibilities offered by ordinary diffractometers and time-of-flight diffractometers.

For brevity, below we shall refer to these two basic types as DA (Double Axes) and TOF (Time-Of-Flight) diffractometers, respectively. It is assumed that the reader is familiar with the problems of neutron diffraction, which are discussed in books and reviews (Refs. 2–5), and the examples of actual studies given here are only illustrative of certain aspects of their realization at pulsed sources.

The numerous and diverse neutron-diffraction studies can be divided into three groups of experiments, the performance of each of which requires a particular diffractometer arrangement. These are:

experiments carried out on polycrystals;
experiments carried out on single crystals;
studies of transient processes in crystalline materials.

The current requirements on TOF diffractometers used for these three types of experiment are listed in Table I. It can be stated that the essential feature of the contemporary TOF diffractometer for studying polycrystals is its high resolution, in the case of single crystals it is the use of a position-sensitive detector (PSD) with good spatial resolution, and for studying transition processes it is high luminosity.

These conditions are discussed in more detail in the corresponding sections of this review after some general questions are considered.

1. SPECIFIC FEATURES OF NEUTRON DIFFRACTION AT PULSED NEUTRON SOURCES

High-flux pulsed neutron sources

The use of the pulsed method of bombarding a sample in neutron diffraction originates in the beam chopper used at stationary reactors. Electron accelerators with breeder targets (Harwell, England, 1958) and the IBR-1 pulsed reactor (Dubna, JINR, 1960) were an important step forward. These sources possessed many useful properties, but in neutron-diffraction experiments they could not seriously compete with powerful stationary reactors. The pre-1975

 0090-4759/92/040481-25$04.00

TABLE I. Requirements on the basic diffractometer characteristics for the realization of three types of diffraction experiment.

Type of experiment	Luminosity	Resolution	Detector system
Polycrystal structure	high	very high	ordinary detector with large solid angle
Single-crystal structure	average	average	one- or two-coordinate PSD
Transient processes	very high	average	multidetector system

developments of different variants of the neutron time-of-flight method—Fermi choppers in a stationary reactor, rotating crystals, pulsed sources, etc.—are described in Refs. 6–9.

The situation changed dramatically after the appearance of the high-flux IBR-2 pulsed reactor[10] at Dubna and several sources based on a proton accelerator with target made of a heavy metal (the spallation neutron source, SNS; Ref. 11). At the present time there are five high-flux pulsed sources (Table II) and several less powerful ones in operation at neutron-study centers around the world.

In the design of a diffraction experiment the most important characteristics of the source are the average flux and the width of the thermal-neutron pulse, and also the pulse repetition rate. The average flux is considerably larger in a pulsed reactor than in an SNS. In all sources the thermal-neutron pulse is formed by some type of moderator, and its shape is the convolution of the fast-neutron pulse and the moderator response function. For sources of the SNS type the width of the fast-neutron pulse is so small that it does not affect the final result; everything is determined by the moderator, which can be optimized either in the neutron yield or in the pulse width.[12] In any case the thermal-neutron pulse obtained is 10–20 times shorter than in a reactor, so that the time resolution can be higher by the same factor.

In principle, pulsed sources can be compared in terms of the parameter $Q=P/W^2$, where P is the average thermal-neutron flux and W is the pulse width, referred to as the "worth," which is interpreted as the flux at the sample for a given time resolution. However, more careful study shows[5] that different parameters Q should be introduced for different types of experiments, in particular, the power of W in the definition can vary between 0 and 3. In addition, in a comparison it is necessary to take into account the actual pulse repetition rate of the source. For example, at a rate of 50 s^{-1} in working with wavelengths in the range from 1 to 5 Å on a path length of 100 m (an HRPD diffractometer at an SNS), four out of five pulses must be passed. Thus, without going into a detailed comparison of the various pulsed sources, it can be stated that for the IBR-2 it is preferable to carry out experiments requiring high luminosity and moderate time-of-flight resolution, while an SNS corresponds better to the requirement of high resolution. However, this conclusion may be somewhat modified when the Fourier technique of recording neutron diffraction patterns is developed further.

Since the difference between experimental setups at pulsed and stationary neutron sources is so great, nothing interesting can be learned by comparing them directly, although an entire chapter of Ref. 5 is devoted to this. Even comparison of the data acquisition rate and the accuracy of the diffraction data for a single sample with the standard improvement of the polycrystalline structure leads only to qualitative conclusions, i.e., owing to the different observed d_{hkl} range and the different behavior of $R(d)$, the situations regarding the position and thermal parameters of the atoms are different (see, for example, Ref. 13, where the data for Al_2O_3 are compared). Experience shows that for TOF and DA diffractometers of the same class, i.e., with roughly identical resolution and total flux on the sample, the worth of the structural information is also roughly the same, while certain details can differ very strongly.

TABLE II. Characteristics of operating high-flux pulsed neutron sources.

Source	Type	Year operation began	I/P	Frequency, s^{-1}	W, μs fast neutrons	W, μs th. neutrons	Average flux density
IPNS ANL, USA	Synchrotron	1981	16 μA	30	0,1	20–30	20
IBR-2 JINR	Reactor	1984	2 MW	5	230	320	800
ISIS RAL, England	Synchrotron	1985	100 μA	50	0,4	20–30	70
LANSCE LANL, USA	Linear accelerator	1988	100 μA	20	0,3	20–30	50
KENS-1 KEK, Japan	Synchrotron	1988	5 μA	15	0,5	30–35	7

Note. The accelerator (synchrotron or linear accelerator) current or the average reactor power are given in the I/P graph. The width of the neutron pulse is given for fast and thermal neutrons. The average flux density is approximate; it is given in units of 10^{10} neutrons/s from 1 cm^2 of the moderator surface.

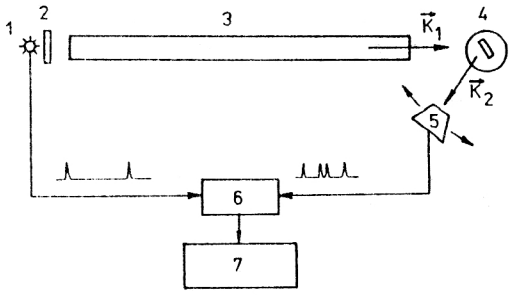

FIG. 1. Functional scheme of the TOF diffractometer: 1—pulsed source, 2—moderator, 3—preliminary path, 4—sample, 5—detector, 6—analyzing device, 7—internal memory.

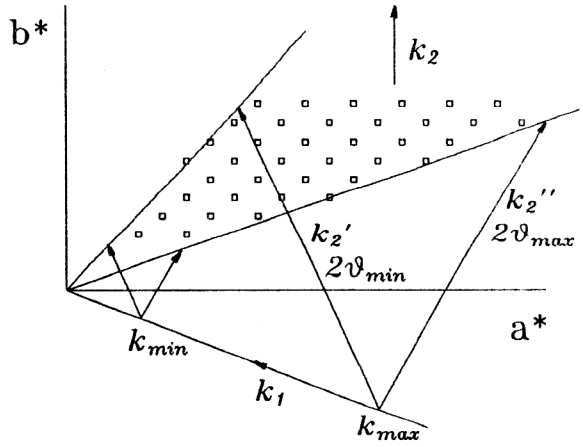

FIG. 2. Region of reciprocal space observed in a TOF diffractometer in the case of a one-coordinate PSD. The (a^*,b^*) section of the reciprocal lattice, the primary beam direction $\mathbf{k}_1$, and the average direction of the scattered beam $\mathbf{k}_2$ are shown. The recording is done in the range of scattering angles from $2\theta_{min}$ to $2\theta_{max}$ (the directions $\mathbf{k}_2'$ and $\mathbf{k}_2''$, respectively) and in the range of neutron wave vectors from k_{min} to k_{max}. The symbols ■ denote the lattice sites falling in the observed region.

Time-of-flight diffractometers

It is well known that a DA diffractometer at a stationary reactor actually copies the x-ray diffractometer scheme: a monochromator directs a narrow ($\Delta\lambda/\lambda \leqslant 0.01$) line on the sample, and a scattering-angle sweep gives the diffraction spectrum. This is done either by scanning an angular range by a single detector or by a multicounter or position-sensitive detector system.

The main features in the design of a neutron-diffraction experiment are considerably different from those of an x-ray experiment. They are the following:

the energy spectrum of thermal neutrons from the reactor has a continuum (Maxwellian) nature;

the thermal-neutron speed is small, and the neutron energy (or wavelength) can be analyzed from the time of flight.

The functional scheme of a TOF diffractometer is shown in Fig. 1. After being slowed down to thermal energies, neutrons from a pulsed source travel along a preliminary path where they are collimated and made monochromatic. They then scatter on the sample and are recorded by a detector at some fixed direction. An analyzing device writes the spectrum to the internal memory with a sweep in the neutron time of flight from the moderator to the detector. The spectra from successive pulses of the source are summed to accumulate the needed statistics. Synchronization of the analyzer with the power pulse of the source is done by means of special starting pulses. The vectors $\mathbf{k}_1$ and $\mathbf{k}_2$ denote the directions of the primary and scattered neutron beams, and their modulus varies continuously in accordance with the time of flight.

The basic parameters of a neutron diffractometer determining the possibilities of the setup and the worth of the experiment, and which can be used to compare diffractometers with each other, are the range of interplanar spacings d_{hkl} accessible to measurement, the total neutron flux at the sample in the working range of wavelengths, Φ_0, and the resolution R. For a diffractometer designed to study polycrystals, additional characteristics are the possible "useful" sample volume V_s, the solid angle of the detector system, Ω_d, and the luminosity J, defined as the product $\Phi_0 V_s \Omega_d$. In addition to the parameters themselves, there are very important functional dependences: the dependence of the resolution on the wavelength and scattering angle, the dependence of the flux on the wavelength, and so on, and also various other possibilities of the diffractometer such as the possibility of measuring the same reflection at different wavelengths.

The main consequences of the changeover to a continuous spectrum and the use of the time-of-flight method for the wavelength sweep of the diffraction picture are well known.

The most important consequence is the many-fold increase of the fraction of neutrons from the source which are used. As a result, in spite of the fact that the time-averaged neutron flux at the existing pulsed sources is considerably smaller than at stationary sources, $\Phi_0 = 8 \times 10^{12}$ for the IBR-2 (JINR) and $\Phi_0 = 1.5 \times 10^{15}$ neutrons/cm^2/s for the HFR (ILL, Grenoble), the diffraction-data acquisition rate is comparable and in some special types of experiment many times higher than in a TOF diffractometer.

The range of wavelengths used at a TOF diffractometer can be very broad. Usually it is 0.9–8 Å, although both very small (down to 0.5 Å) and very large (up to 20 Å) wavelengths are also used. This makes it possible to cover a wide range of interplanar spacings by using a small number of detectors. Actually, only two detectors located at scattering angles of 20° and 160° allow observation of d_{hkl} in the range from 0.46 to 23 Å when working in the range $0.9 \leqslant \lambda \leqslant 8$ Å, according to the Bragg law $d = \lambda/(2 \sin \theta)$.

Two- or three-dimensional diffractometry of the reciprocal space of a crystal is easily realized using a TOF diffractometer. The time of flight gives the sweep along the radius vector of the reciprocal lattice, and the position groups of a one- or two-coordinate position-sensitive detector give the sweeps in the transverse directions (Fig. 2).

The resolving power of a TOF diffractometer for polycrystals can easily be reduced to $\Delta d/d = 0.003$ and even to

0.0005 in special cases; it is nearly or completely independent of d_{hkl}.

Traditionally accepted features of the TOF diffractometer are also the possibility of carrying out measurements in a fixed geometry, which is important, for example, in working with high-pressure chambers, and the pulsed nature of the bombardment of the sample by the neutron beam. The latter also allows external action on the sample to be realized in the pulsed mode, owing to which the amplitude of this action can be increased greatly.

An important deficiency of the TOF diffractometer is the fact that the precision of the data obtained with it is lower than usual. This is related to the need to introduce a large number of wavelength-dependent corrections in the transformation of the measured intensities of the diffraction peaks into structure factors. The most important of these is the effective spectrum of neutrons incident on the sample, which includes transmission on the path lengths and the detector efficiency. This correction can vary by factors of ten, depending on the wavelength. The methods of determining it are not yet perfect, and it is what largely determines the accuracy of the experimental values of the structure factors of the crystal.

Determination of the structure factors of a crystal using a TOF diffractometer

A. Dependence of the intensity of the diffraction spectrum on λ and θ

In a neutron-diffraction experiment the intensity I of neutrons scattered on the sample is measured. This in general is a three-dimensional function of the momentum transfer and is related to the cross section σ for scattering on the sample by a convolution type of integral:

$$I(\mathbf{Q}_0)=\int R(\mathbf{Q}-\mathbf{Q}_0)\sigma(\mathbf{Q})d\mathbf{Q}, \tag{1}$$

where R is the three dimensional resolution function of the diffractometer, $\mathbf{Q}_0=\mathbf{k}_2-\mathbf{k}_1=2\pi\mathbf{H}$ is the momentum transfer, $\mathbf{k}_1$ and $\mathbf{k}_2$ are the neutron wave vectors before and after the scattering, and $\mathbf{H}$ is a vector in the reciprocal space of the crystal. The actual expression for $I(\mathbf{Q}_0)$, like the methods of extracting the structural information, depends on the type of sample and the particular problem.

The most common goal of a structure experiment on a single crystal is the construction of the Fourier series for the scattering density:

$$\rho(\mathbf{r})\sim\sum_{hkl}F(\mathbf{H})\exp(-2\pi i\mathbf{Hr}), \tag{2}$$

where $\mathbf{H}\equiv\mathbf{H}_{hkl}$ is a discrete set of reciprocal lattice vectors and F is a structure factor related to the coherent cross section for neutron scattering by a unit volume of the crystal:

$$\sigma(\mathbf{Q})=\frac{(2\pi)^3}{V_c^2}|F(\mathbf{H})|^2\varphi(\mathbf{Q}-2\pi\mathbf{H}), \tag{3}$$

where V_c is the volume of the elementary cell of the crystal and the function φ determines the shape and size of the sites of the reciprocal lattice. It depends, for example, on the distribution in the orientations of the mosaic blocks making up the crystal, the dispersion of the interplanar spacings, and so on. In the case of an ideal crystal φ can be assumed to be a δ function.

The usual method of determining $|F(\mathbf{H})|$ is integration of $I(\mathbf{Q}_0)$ over all $\mathbf{Q}_0$ contributing to the intensity of the peak. This procedure makes it possible to get rid of the frequently unknown resolution function, i.e.,

$$\int I(\mathbf{Q}_0)d\mathbf{Q}_0=\iint R(\mathbf{Q}_0-\mathbf{Q})\sigma(\mathbf{Q})d\mathbf{Q}d\mathbf{Q}_0$$

$$=\text{const}\int\sigma(\mathbf{Q})d\mathbf{Q}. \tag{4}$$

The constant in this expression is determined by the conditions under which the reciprocal space is scanned, and for the TOF diffractometer (stationary sample) the relation between the integrated intensity and the structure factor is given by the familiar expression

$$I_{\text{int}}=\int I(\mathbf{Q}_0)d\mathbf{Q}_0$$

$$=\Phi(\lambda_0)V_s\frac{\lambda_0^4|F|^2}{2V_c^2\sin^2\theta_0}A(\lambda_0,\theta_0)y(\lambda_0,\theta_0), \tag{5}$$

where Φ is the spectral density of the neutron flux at the sample, V_s is the crystal volume, A and y are the corrections for absorption and extinction, and λ_0 and θ_0 are the wavelength and Bragg angle at which the diffraction peak is measured.

In obtaining (5) we have used the condition that the distribution $I(\mathbf{Q}_0)$ is narrow, i.e., only in this case is it possible to take the functions Φ, A, and y out of the integral because they vary weakly within the peak. This condition is almost always satisfied; it can only be violated in the case of long-period structures, which are being studied more and more often using TOF diffractometers.

Another common problem is the analysis of the shape of the reciprocal lattice sites, i.e., measurement of $\sigma(\mathbf{Q})$. In this case it is desirable to have as narrow a resolution function as possible, a δ function in the limit, so that $I(\mathbf{Q})\sim\sigma(\mathbf{Q})$ holds. To measure $\sigma(\mathbf{Q})$ it is necessary to vary the argument of the function φ, i.e., the reciprocal space must be scanned. In a TOF diffractometer the scanning can be done by varying five parameters: the neutron wavelength and the directions of the vectors $\mathbf{k}_2$ and $\mathbf{H}$. For example, if a two-coordinate PSD is used to detect the scattered neutrons, scanning in the wavelength and the direction of $\mathbf{k}_2$ is done automatically. The choice of a specific scanning region is made by orienting the crystal appropriately (choice of the direction of the vector $\mathbf{H}$ relative to $\mathbf{k}_1$).

As yet another variant of analyzing Eq. (1) let us consider the problem of the structural analysis of polycrystalline matter. In this case the scattering cross section (3) must be averaged over the orientations of the vector $\mathbf{H}$, which leads to the expression

$$\sigma(Q)=\frac{(2\pi)^2}{V_c^2 H^2} j|F|^2\varphi(Q-2\pi H), \qquad (6)$$

where j is the repetition factor and the function φ now describes the shape of the site after projection of the original distribution onto the radius vector $\mathbf{H}$. To measure σ it is sufficient to scan the reciprocal space in the neutron wavelength, after which it becomes possible to write the measured diffraction spectrum as

$$I(d)=C\Phi(d)A(d)\sum_n j_n|F_n|^2 d_n^4 m(d_n-d), \qquad (7)$$

where $d=\lambda/2\sin\theta$ is the interplanar spacing, C is a normalization constant containing all the factors independent of d, A is the absorption factor, and n stands for the triplet of Miller indices (hkl), i.e., the sum runs over all peaks contributing to the measured spectrum. In addition, m is a function describing the shape of the diffraction peaks; for an ideal polycrystal it coincides with the diffractometer resolution function. It is also possible to include the extinction and grain structure of the sample in (7). The main difference between (5) and (7) and the corresponding expressions for the case of a DA diffractometer reduces to the appearance of dependences of the functions Φ, A, and y on the neutron wavelength, the correct inclusion of which is extremely important in precision structure experiments. Let us consider these dependences in more detail.

B. Inclusion of the effective neutron spectrum

The function Φ is understood as the effective neutron spectrum Φ_e, i.e., the spectral density of the flux in the primary beam including η, the neutron transmission on the path lengths before and after scattering, and μ, the detector efficiency: $\Phi_e(\lambda)=\Phi(\lambda)\eta(\lambda)\mu(\lambda)$. If Φ_e is defined in the geometry standard for a diffraction experiment and with the same detector, independent measurement of Φ, η, and μ is not required. The most common method of measuring Φ_e is use of an incoherent scatterer, usually vanadium, the differential cross section for elastic incoherent scattering of which, σ_{inc}, is treated as isotropic and independent of the neutron wavelength. In fact, there also are weak dependences both on the scattering angle and on λ, and, in principle, they must be taken into account. The following procedure can be used for this.[14]

Usually in the vanadium experiment the scattered neutrons are not analyzed in energy, so that rather than measuring the scattering differential cross section, the integral of the doubly differential cross section modulated by the primary beam along the curve $t_1+t_2=t_0$ is measured. Here t_1 and t_2 are the times of flight before and after the scattering, and t_0 is the time of flight of elastically scattered neutrons. In this case the intensity

$$I(E_0,\theta)\sim\sigma_{\text{inc}}e^{-2W}\Phi(E_0)+\frac{L}{L_2}\int_{E_\psi}^{\infty}\Phi(E_1)\times(\psi E_1/E_0)^{3/2}\sigma(E_1,\theta)dE_1 \qquad (8)$$

is recorded, where E_0 is the energy of the elastically scattered neutrons, E_1 and E_2 are the energies corresponding to the times t_1 and t_2, e^{-2W} is the Debye–Waller factor of vanadium, L_1 and L_2 are the neutron paths before and after scattering, $L=L_1+L_2$, $E_\psi=E_0L_1^2/L^2$, the function $\psi=L_2^2/[L(E_1/E_0)^{3/2}-L_1]^2$ and the final energy $E_2=E_1\psi$ are determined from the condition $t_1+t_2=t_0$, and $\sigma(E_1,\theta)$ is the doubly differential scattering cross section for vanadium, including the incoherent and inelastic components. The solution of this integral equation for $\Phi(E)$ can be simplified considerably by assuming that $L_2\ll L_1$, which is valid for most TOF diffractometers. Here (8) can be rewritten as

$$I(E_0,\theta)=c\xi(E_0,\theta)A(E_0,\theta)\Phi(E_0), \qquad (9)$$

where c is a normalization constant, ξ is a correction factor equal to the ratio of (8) and $\Phi(E_0)$, and A is the usual absorption factor. Since ξ differs little from unity, it can be calculated using the Maxwell approximation for Φ and any approximate expression for the doubly differential cross section. The dependence of the correction factor on λ is shown in Fig. 3 for the DN-2 diffractometer (JINR). We see that the correction is important in a rather wide range of wavelengths, although it does not exceed 10%. The correction of the spectrum at small λ and large scattering angles requires special treatment.

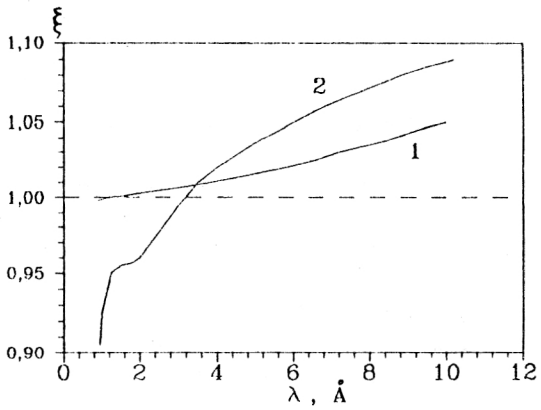

FIG. 3. Dependence of the correction factor ξ in Eq. (9) on the neutron wavelength for two scattering angles: (1) 10°, (2) 145°.

Scattering on vanadium can actually be used to calibrate the spectrum up to wavelengths of 8 Å; at higher ones the effect-to-background ratio becomes too small. This limit can be raised by using diffraction on a polycrystal having diffraction peaks at large wavelengths, and for $\lambda>12$ Å the spectrum can be measured by mirror reflection of neutrons. An $Fe(CN)_6K_3$ polycrystal and an Ni mirror were used for this in the DN-2 TOF diffractometer. After measuring the spectra from the vanadium, the mirror, and the polycrystal and jointly analyzing all the data, it proved possible to cover the entire required range of wavelengths from 0.7 to 22 Å (Ref. 14).

C. Inclusion of absorption and extinction

The initial expressions for these corrections are exactly the same as for the case of the DA diffractometer. The

absorption factor is included by calculating the integral over the sample volume,

$$A(\lambda,\theta)=\frac{1}{V}\int \exp(-\mu\xi)dV, \qquad (10)$$

where $\mu=\mu(\lambda)$ is the linear attenuation coefficient depending on the neutron wavelength and ξ is the neutron path in the sample. For all the elements except hydrogen and several isotopes which strongly absorb neutrons (^{113}Cd, ^{149}Sm, ^{155}Gd,...) only the absorption cross section depends on the wavelength:

$$\mu(\lambda)=\sum n_i(\sigma_{\text{inc}}+\sigma_{\text{abs}}\lambda/\lambda_0)_i, \qquad (11)$$

where n_i is the number of atoms of type i per unit volume, σ_{inc} and σ_{abs} are the cross sections for incoherent scattering and absorption, the sum runs over all the atoms in the elementary cell, and λ_0 is the wavelength at which the value of the absorption cross section is taken. As is well known, the cross section for the incoherent elastic scattering of neutrons by hydrogen varies from 20 to 80 b, depending on the strength of its coupling in the structure and the incident-neutron energy. The following approximation was suggested for it in Ref. 15:

$$\sigma_{\text{H-inc}}\approx 35.2+12(\lambda-1)\text{b}, \qquad (12)$$

with λ in Å. This dependence is accurate for wavelengths in the range from 0.7 to 3.0 Å for organic compounds and hydrates. In other cases it is necessary to introduce an empirical correction for absorption in a sample containing hydrogen.

For the isotopes listed above, which have a strong resonance at thermal energies, not only the absorption but also the coherent scattering length depends on the wavelength, also in a resonance manner (see, for example, Ref. 16). This must be given special treatment.

The analysis carried out in Ref. 17 showed that to correct the intensities measured using a TOF diffractometer for the extinction effect it is not necessary to reformulate the Zachariasen, Cooper–Rouse, or Bekker–Kopens algorithms widely used for the DA diffractometer. There is no doubt that the most recent algorithm developed in Ref. 18 and eliminating some defects of the Bekker–Kopens method can also be used.

The algorithm which is simplest and in addition has a pronounced dependence of the extinction coefficient on the wavelength is the Zachariasen algorithm,[19] which, for example, for the case where there is only secondary extinction, leads to the expression

$$y(\lambda,\theta)=[1+2rQ_0T/\lambda\sqrt{1+(r/\lambda g)^2}]^{-1/2}, \qquad (13)$$

where $Q_0=\lambda^3F^2/(V_c^2\sin 2\theta)$, T is the average neutron path in the sample, and r and g are parameters corresponding to the radius of the mosaic blocks of the crystal and their degrees of disorientation [$g=1/(2\sqrt{\pi\eta})$, where η characterizes the mosaic structure of the sample]. For two limiting types of crystal, (I) where $r\gg g\lambda$ and (II) where $r\ll g\lambda$, for $y(\lambda,\theta)$ we find

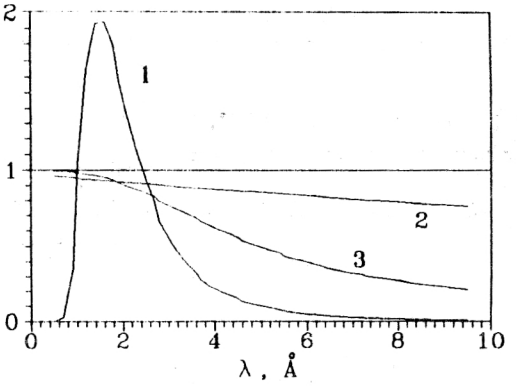

FIG. 4. Wavelength dependence of the three main corrections introduced into the measured intensities in transforming to the structure factors: (1) effective neutron spectrum, (2) absorption factor, (3) extinction coefficient.

$$\text{(I)}\quad y(\lambda,\theta)=[1+2gQ_0T]^{-1/2},$$

$$\text{(II)}\quad y(\lambda,\theta)=[1+2rQ_0T/\lambda]^{-1/2}. \qquad (14)$$

We see that the extinction coefficient always decreases rapidly with increasing wavelength. In Fig. 4 we show (in a typical case) how the functions Φ, A, and y depend on the wavelength. Obviously, the most serious problem is the inclusion of the effective spectrum. However, it should be noted that the incorrect inclusion of these corrections in going from the intensities to the structure factors primarily affects the thermal parameters of the atoms and the occupation factors.

2. STRUCTURE STUDIES OF POLYCRYSTALS

A schematic diagram of a contemporary TOF diffractometer for measuring neutron powder diffraction is shown in Fig. 5. It is characterized by a relatively large path length L from the moderator to the sample to ensure good time-of-flight resolution, which is always $\sim L^{-1}$, and several detectors of large area. The chopper-filter eliminates from the beam background neutrons from the source, including neutrons from one or several basic pulses if it is necessary to lower their frequency. A mirror curved neutron guide tube is almost always used as the principal element for forming the thermal-neutron beam at the sample. This makes it possible to greatly decrease the intensity losses due to the large flight path and, moreover, it plays the role of a filter eliminating fast neutrons and γ rays from the source in the beam. The principal high-resolution detector is stationary and located in the position corresponding to the largest possible scattering angle. The auxiliary detectors can also be stationary or located on platforms rotating about the central axis of the diffractometer. The heating elements, cryostats, and other devices are located in the massive central bollard.

Resolution of the TOF diffractometer for polycrystals

In the one-dimensional case of a time-of-flight diffraction spectrum the resolution is usually expressed as

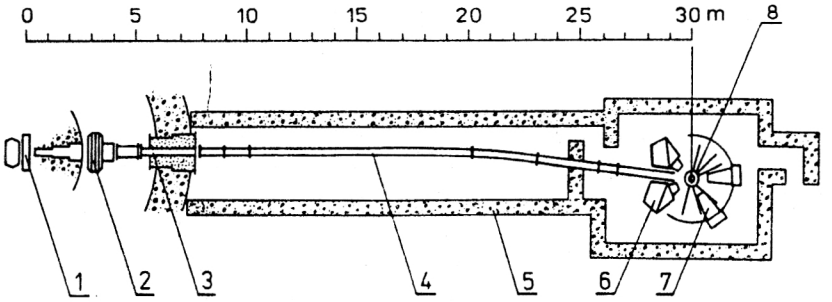

FIG. 5. Schematic diagram of the TOF detector: 1—neutron moderator, 2—mechanical chopper-filter, 3—channel inside the biological shielding wall around the source, 4—curved mirror neutron guide tube, 5—biological shielding of the diffractometer, 6—high-resolution detector, 7—auxiliary detector, 8—sample site.

$R=\Delta d/d$, where d is the interplanar spacing. In the lowest-order approximation it is given by two terms:

$$R=\Delta d/d=[(\Delta t/t)^2+(\Delta\theta/\tan\theta_0)^2]^{1/2}, \qquad (15)$$

where t is the total time of flight from the moderator to the detector, θ_0 is the Bragg angle, Δt takes into account the uncertainties in the time of flight, which primarily come from the width of the primary neutron pulse and also the width of the time-analyzer channel, the uncertainty in the detection point, and so on, and $\Delta\theta$ includes the geometrical uncertainties of the scattering process. Here and below quantities labeled Δ will correspond to the full width at half-max of the corresponding distribution function.

The time-of-flight part of the resolution function (denoted by R_t) can be written as

$$R_t=\Delta t/t=\Delta t/(252.778L\lambda), \qquad (16)$$

where Δt, L, and λ are expressed in μs, m, and Å, respectively. At pulsed sources of the SNS type with a short ($\leqslant 1$ μs) pulse of fast neutrons the quantity Δt is mainly determined by the construction of the moderator. If the exit layer (after the Cd disk) of the moderator is less than 15 mm, then $\Delta t\approx 10\lambda$ μs if λ is expressed in Å. In this case R_t depends weakly or not at all on λ, and already at $L=20$ m the level $R_t\leqslant 0.002$ can be reached; this is typical of a high-resolution diffractometer.

In the simplest case of an unfocused system the geometrical part of the resolution function R_θ is determined by the collimation of the primary and scattered beams, γ_1 and γ_2, respectively:

$$R_\theta=\Delta\theta/\tan\theta_0=(\gamma_1^2+\gamma_2^2)^{1/2}/\tan\theta_0, \qquad (17)$$

if the contribution from the sample is neglected. When the primary beam is formed using a mirror neutron guide tube, $\gamma_1=\gamma_c$, where γ_c is the critical reflection angle; for example, for an Ni coating it is $\gamma_c=0.00173\lambda$ rad$=5.95\lambda$ arc min, with λ in Å. We see that if the diffraction spectrum is measured at the scattering angle 90°, it is necessary to use a Soller exit collimator, so that R_θ remains at the level 0.002 for $\lambda\geqslant 1$ Å. For the second term in $\Delta\theta$ we have $\gamma_2=l_d/2L_2$, where l_d is the visible dimension of the detector or the width of the position group if a PSD is used and L_2 is the distance from the sample to the detector. The actual value of l_d is 0.5 cm, and then it is necessary to have $L_2\geqslant 150$ cm to preserve the high resolution.

The above expression for R_θ is valid if the characteristic dimensions of the moderator and the detector are small, and their surfaces are perpendicular to the average paths in the primary and scattered beams. When they are not perpendicular, terms containing $\Delta L/L$ and, accordingly, $\Delta t/t$ appear. As a result, the so-called time-focusing conditions[20] can be realized. Here the angles of the moderator α_1 and the detector α_2 must satisfy the equations

$$2\frac{L_1}{L}\tan\alpha_1\tan\theta_0=1, \quad 2\frac{L_2}{L}\tan\alpha_1\tan\theta_0=1. \qquad (18)$$

When these conditions are satisfied, the geometrical term is eliminated from (15) in the lowest-order approximation. In general, it is multiplied by some factor which takes into account the decrease of R_θ when the time-focusing conditions are completely or partly satisfied.

Calculations show that a diffractometer constructed with allowance for the focusing of only the detector system has, for small samples, a luminosity about five times larger than when Soller collimators are used. In practice, it is best to use a partially focused system, such that the contributions R_t and R_θ in the resolution function are equal. This gives the best compromise between the luminosity and the resolution.

The maximum resolution of the TOF diffractometer

When the scattering angle increases, R_θ decreases as $\cot\theta_0$, and for $\theta\geqslant 85°$ and large L the resolution of the TOF diffractometer can be increased considerably. To illustrate the improvement of the resolution, in Fig. 6 we show the result of a model calculation of a small segment of the diffraction spectrum for a $YBa_2Cu_3O_7$ polycrystal for $R=0.010$ and with R decreased by factors of 4 and 16. It is clearly seen how large is the detail that can be observed in the last case. An example of a setup with resolution close to the maximum is the HRPD diffractometer[21] at the Rutherford Appleton Laboratory in England, which began operation in 1986. At the HRPD it was possible to improve the resolution by a factor of 5 to 7 compared with existing diffractometers, and the limit $\Delta d/d=0.001$ was exceeded for the first time in neutron diffraction. This was achieved by increasing the flight path from the moderator to the sample to 96 m and installation of a ring backscattering detector covering the angles 170° to 178°. Owing to the geometrical contribution, $\Delta d/d$ varies slightly from ring to ring, gradually decreasing with increasing angle and wavelength. The value of the resolution averaged over the entire detector is 0.0005 for $d=2$ Å. Data from the individual rings of the detector are accumulated independently, and

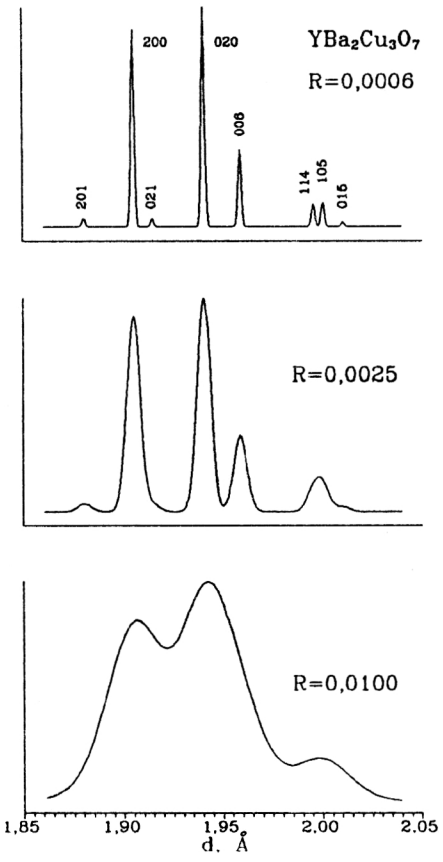

FIG. 6. Model calculation of the diffraction spectrum of $YBa_2Cu_3O_7$ in the region $d=2$ Å for various diffractometer resolutions: $R=0.01$, 0.0025, and 0.0006.

later the spectra are summed, taking into account the shift of the peak positions according to the Bragg law ("electronic focusing").

Experience with the operation of the HRPD has shown that for a resolution better than 0.001 it actually becomes possible to solve qualitatively new problems, for example, the *ab initio* powder structure analysis, observation of the anisotropic broadening of diffraction lines, and also observation of lattice excitations without energy analysis.

The Fourier diffractometer for studying polycrystals

The neutron Fourier diffractometer is a new and very specific stage in the development of high-resolution neutron powder diffraction. At present, in the whole world there are two Fourier diffractometers operating at stationary reactors, SFINKS at the St. Petersburg Nuclear Physics Institute (Gatchina, Russia) and FD at GKSS (Geesthacht, Germany), and one diffractometer operating at a pulsed neutron source, the HRFD at the JINR. Since independently of the source these installations are TOF diffractometers and moreover are very promising, we shall discuss them in this review.

The closest analogs of the Fourier diffractometer (henceforth referred to as the F diffractometer) are setups with a Fermi chopper in a stationary reactor, which became somewhat widespread in the 1960s. However, with the appearance of pulsed neutron sources these gradually went out of use. The simplest variant of a Fermi chopper is a disk with a single slit transparent to neutrons. Sufficiently high resolution is obtained, owing to the narrowness of the slit and the high rotation frequency of the disk. The beam-use coefficient is determined by the ratio $l_s/2\pi R_c$, where l_s is the slit width and R_c is the disk radius. This coefficient is less than 0.01. The situation can be improved by using two or more slits, but here the working range of wavelengths is decreased proportionally, owing to the overlap of the spectra from separate pulses. The beam chopper used in the F diffractometer (the F chopper) is a limiting case of a Fermi chopper with several slits, in which the widths of the slit and the nontransmitting section are equal, the disk is uniformly filled with slits (there are about 10^3 of them), and the diffraction spectra due to pulses from adjacent slits overlap almost completely. It turns out that a new feature appears in this limit: it becomes possible to identify the overlapping spectra by a specially organized measurement process.

The Fourier diffractometer[22] at the stationary reactor of the St. Petersburg Nuclear Physics Institute (in operation since 1984) has proved to be quite competitive and has demonstrated both the correctness of the main ideas on which it is based and the high quality of the results obtained. A particular defect of the F diffractometer in a stationary neutron source is the high level of the correlation background, which makes it difficult to record diffraction peaks in low-intensity regions of the neutron spectrum, in particular, at large wavelengths. In Refs. 23 and 24 it was shown that the use of an F-diffractometer setup at a pulsed source leads to significant improvement of the effect-to-background ratio and ensures high acceptance and very high (at the level $\Delta d/d=0.0005$) resolution.

The recording of the spectra is based on the use of special RTOF (Reverse Time-Of-Flight) correlators realizing the idea of the inverse Fourier method[25] for identifying overlapping diffraction spectra. The method amounts to analysis of the situation preceding the detection of the neutron. Owing to the overlap of the spectra, it is impossible to know exactly what was the velocity of the neutron recorded by the detector, but it is possible to know what velocities it could have had by checking the state of the chopper and the reactor at earlier times. It turns out that by varying the chopper rotation frequency from zero to some maximum value and accumulating a large number of events sorted in this manner, it is possible to obtain the usual spectrum of elastically scattered neutrons with a time sweep. The possibility of sorting is ensured by the formation of reference signals coinciding with the times at which the reactor and chopper are in the "open" state and controlled by the operation of a fast shift register via which the detector signals are collected.

In the case of the standard TOF diffractometer the time dependence of the intensity recorded by the detector of neutrons elastically scattered on the sample (a one-dimensional time-of-flight spectrum) can be written as the sum of two terms:

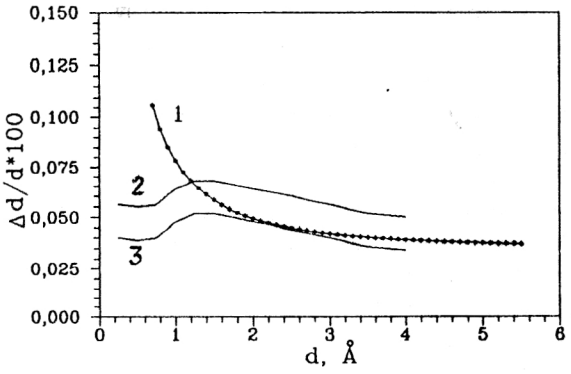

FIG. 7. Comparison of the resolution functions for the HRFD (curve 1) and HRPD diffractometers. For the HRPD the curves corresponding to the inner (3) and outer (2) rings of the detector are shown.

$$I(t)\sim\int R(\xi-t)\sigma(\xi)d\xi+B(t), \tag{19}$$

where σ is a function proportional to the scattering cross section (6) (for an ideal polycrystal this is a sum of δ-function distributions corresponding to the Bragg diffraction peaks), R is the resolution function of the setup, and B is the statistical background. The analogous expression for the Fourier diffractometer at a pulsed source is

$$I(t)\sim\int R(\xi-t)R_c(\xi-t)\sigma(\xi)d\xi + \int R(\xi-t)\sigma(\xi)d\xi+B(t), \tag{20}$$

where R_c is a function related to the neutron-beam modulation effect. It can be shown that in the first approximation

$$R_c(t)\sim\int_0^{\Omega_m} g(\omega)\cos(\omega t)d\omega, \tag{21}$$

where $g(\omega)$ is the frequency distribution function of the F chopper and Ω_m is the maximum modulation frequency of the neutron beam. In the first approximation, for example, for the Blackman frequency window used at the SFINKS spectrometer,

$$g(u)=1+p\cos(\pi u)+q\sin(\pi u), \tag{22}$$

where $u=\omega/\Omega_m$, $p=1.03$, $q=0.08$, with the width of the resolution function $W_c\sim\Omega_m^{-1}$. For $N=1024$ slits and maximum rotation frequency of the F-chopper disk $\omega_m=9000$ rev/min the modulation frequency is $\Omega_m=N\omega_m=150$ kHz, so $W_c\approx 7$ μs. If the time-of-flight distance from the F-chopper disk to the detector is $L=20$ m (as in the HRFD case), then for $d=2$ Å the relative contribution of W_c to the full resolution function is $\Delta t/t=0.00033$. The existence of a geometrical contribution of about the same magnitude leads to a resolution of $\Delta d/d=0.0005$ for the HRFD. In contrast to the TOF diffractometer at an SNS, the width of the neutron pulse at the HRFD is independent of the wavelength, so the behavior of $R(d)$ for the HRFD and, for example, for the HRPD is quite different (Fig. 7).

Analysis of Eq. (20) shows that the spectrum measured using the F diffractometer at a pulsed source consists of narrow diffraction peaks (the first term) superimposed on maxima of width W equal to the width of the source pulse ($W=320$ μs for the IBR-2), which in this case are correlation background (for the F diffractometer at a stationary reactor, W includes the entire operating range of wavelengths). The increase of the statistical spread of the points due to the correlation background, which for each point is roughly equal to the intensity in the range $(-W/2,+W/2)$ about the point, is also a fundamental difference between the F diffractometer and the ordinary TOF diffractometer with the same resolution. To compensate for this effect, the level of statistics accumulated using an F diffractometer must be increased. For example, in the observation of two closely spaced peaks of equal intensity the diffraction pictures recorded by the F and TOF diffractometers will be equivalent if the F spectrum is measured with twice the statistics.

The situation gets worse when observing closely spaced peaks with strongly differing intensity. To qualitatively compare the F and TOF diffractometers it is necessary to introduce the coefficient $k_{\rm cor}$ showing how many times the luminosity of the F diffractometer must be increased for the recorded spectra to be equivalent. Estimates and experience using the SFINKS show that $k_{\rm cor}\approx 100$ for a stationary reactor and $k_{\rm cor}\approx 10$ for a pulsed source. These values seem large at first glance, but a large average reactor flux and the possibility of significantly decreasing the path length allow the losses due to the correlation background to be made up easily. Moreover, at pulsed sources with a broad initial pulse, only the Fourier method can ensure such a radical improvement of the resolution (up to $\Delta d/d=0.0005$, i.e., by a factor of 30 at the IBR-2) for a moderate loss of luminosity. Actually, improvement of the resolution due to increase of the source–sample path length would lead to a decrease of the luminosity of the diffractometer at the IBR-2 proportional to the square of the distance, i.e., by almost a factor of 10^3.

The processing of neutron diffraction patterns from polycrystals

In analyzing the diffraction spectra from polycrystals, the lattice parameters are usually determined and the structural characteristics of the atomic coordinates, the occupation factors, and the thermal parameters are improved. When diffractometers with very high resolution are used, it is also possible to analyze the shape of the diffraction peaks.

The routine method of analysis at present is the Rietveld method, formulated in 1969 (Ref. 26) and much discussed elsewhere.[27,28] In this method a parametric description is introduced for the measured spectrum, which makes it possible to use the method of least squares to determine all the interesting characteristics. The problem thus reduces to minimization of the functional

$$\chi^2=\sum_i \omega_i[J(d_i)-I(d_i)]^2, \tag{23}$$

where ω_i is the weight of the ith point, J is the intensity measured and corrected for the effective spectrum and absorption in the sample, and I is the intensity calculated from an expression analogous to (7):

$$I(d_i)=C\sum_n j_n|F_n|^2 d_n^4 m(d_n-d_i)+I_b(d_i), \tag{24}$$

where d_i is the coordinate of a point expressed on the scale of interplanar spacings, C is a normalization constant, and I_b is the background intensity. All the characteristics of the atoms of the crystal enter into the structure factors F_n, which in the approximation of isotropic thermal oscillations are calculated in the usual manner:

$$F_n=\sum_j r_j b_j \exp[2\pi i(hx_j+ky_j+lz_j)] \times\exp(-B_j/8d_n^2), \tag{25}$$

where the nth peak is determined by the triplet of Miller indices (h,k,l), the sum runs over all independent atoms of a cell, r_j is the factor determining the number of atoms of type j in a cell (if needed, it is a parameter taking into account the occupation of a position by the jth atom), b_j is the coherent scattering length, (x_j,y_j,z_j,B_j) are the coordinates and thermal parameter of the ith atom, and i in this expression is the imaginary unit. The position of the nth diffraction peak is determined by d_n, for which we have

$$d_n=DL\sin(\theta_0+\theta')/H_n+d', \tag{26}$$

where D is a known constant including the coefficient for transforming the spectrum from the time-of-flight scale to the scale of interplanar spacings (the d scale), L is the total path length from the source to the detector, and θ' and d' are parameters used to take into account the possible shifts of the zero of the Bragg angle and the origin of the d scale. The parameters of the elementary cell of the crystal enter into the moduli of the reciprocal-lattice vectors H_n in the usual manner. The parameters L and θ' are improved by calibrating the diffractometer using a standard sample with well known characteristics. To determine them separately it is necessary to carry out measurements at several scattering angles. When improving the parameters of the elementary cell of a crystal, L and θ' must be fixed.

Another group of parameters involved in (24) is the set of parameters used to approximate I_b. In many cases a polynomial of second or sometimes third degree is sufficient for including the background. For samples with large incoherent scattering a term proportional to the effective spectrum is added to I_b.

A question requiring special consideration for the TOF diffractometer is the shape of the diffraction peak. For an ideal polycrystal it is determined by the diffractometer resolution function, which can be measured or specified analytically using several parameters. In this case it enters into the complete set of parameters describing $I(d)$ according to Eq. (24). It should be noted that, in general, the shape of the peak for the TOF diffractometer is more complicated than for the DA diffractometer, and a single point of view regarding its description has not yet been formulated.

For example, at the Argonne Laboratory (United States) an analytic approximation is used for the shape of the peak.[13] This can be obtained by assuming that the response of the moderator to a fast-neutron pulse is described by a function consisting of increasing and decreasing exponentials, and then convolving this function with a Gaussian taking into account the fast-neutron contribution, the geometrical uncertainties, the spread in the detection point, the analyzer channel width, and so on. The resulting function is

$$m(z)=Ae^{-bz^2}\left[F\left(\frac{\alpha+2bz}{2z}\right)+F\left(\frac{\beta-2bz}{2z}\right)\right], \tag{27}$$

where $F(y)=\exp(y^2)\mathrm{erf}(y)$, $z=d_i-d_0$, A, b, α, and β are parameters, and $\mathrm{erf}(y)$ is the error function. Although it is mathematically complicated, it gives a good description of the actual peak shape if the sample contribution is small.

Another variant is to split the peak into three regions, the first two of which are Gaussians with different widths and the third is an exponential tail. The normalizations of these functions are chosen so as to obtain smooth transitions between the regions. This description is used, in particular, for the spectra measured at the KENS source.[29]

Finally, at the HRPD diffractometer[21] (Rutherford Appleton Laboratory) the Ikeda–Carpenter function[30] is convolved with a Gaussian and a Lorentzian or a pseudo-Voigtian, which aids the adequate inclusion of the sample contribution.

In principle, the most reliable method of describing the resolution function is the use of the experimentally measured distribution, for example, in the form of a single intense diffraction peak. This distribution can then be used as a model $m(x)$ which is transformed into a real peak using some functional relation $P(x)=Tm(x)$, where T is the transformation operator. One of the simplest possible transformations is[31]

$$P(x,Q)=Tm(x)=Am\left(\frac{x-P}{kx+W}\right), \tag{28}$$

where the set of parameters Q includes the peak amplitude A, its position P, and peak width varying linearly with coordinate. The use of the transformation (28) presupposes that aside from A, P, k, and W no other characteristics of the peak shape depend on x. This condition is usually well satisfied; at least, it is always possible to split the full spectrum into segments inside which it holds with the required accuracy.

Fairly serious problems arise when the sample contribution is significant and, in addition, is anisotropic, i.e., peaks with different (hkl) in general have different shapes, and often the broadening of the peaks does not display any clear dependence on (hkl). Naturally, this effect mainly arises in diffractometers with $R\leqslant 0.001$. As a way out, it has been suggested that the integrated intensities of the peaks be determined at large d, where the peaks are far apart, and the profile analysis be done at small d, where the effects of the broadening are not so pronounced.

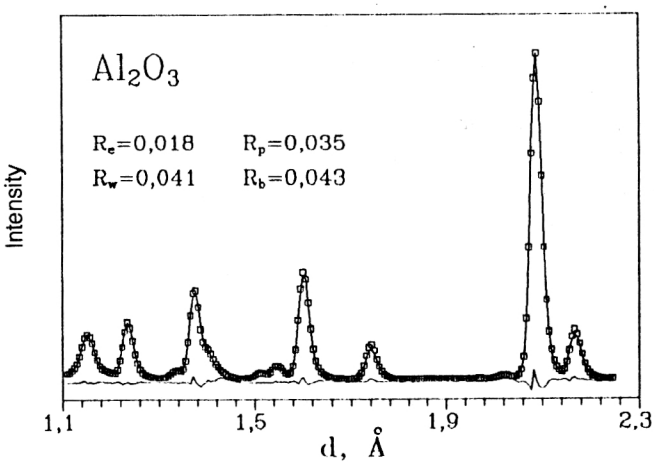

FIG. 8. Segment of the diffraction spectrum of Al_2O_3 measured at the DN-2 diffractometer. The experimental points and curve calculated using the Rietveld method are shown. The difference curve is at the bottom. The values of the R factors characterizing the level of statistics, the background, and the worth of the analysis are given.

Commonly used criteria for the quality of the analysis of diffraction spectra by the Rietveld method are the so-called R factors:

$$R_p = \sum |J_i - I_i| \Big/ \sum J_i,$$

$$R_\omega = \left(\sum \omega_i (J_i - I_i)^2 \Big/ \sum \omega_i J_i^2 \right)^{1/2},$$

$$R_b = \sum |J_i - I_i| \Big/ \sum |J_i - I_{bi}|,$$

$$R_e = \sum D_i^{1/2} \Big/ \sum J_i,$$

where, as before, J_i and I_i are the values of the intensity at the ith point of the spectrum measured and calculated using (24), ω_i is the weight of the point, and D_i is the statistical dispersion for J_i. Here R_e is called the statistical R factor and characterizes the average level of the accumulated statistics (the average relative error). If the proposed model of the structure corresponds ideally with experiment and there are no systematic errors, R_p (the total R factor from the profile) and R_ω (the weighting R factor from the profile) must be roughly equal to R_e. Finally, R_b (the total R factor from the profile with the background subtracted) characterizes the level of excess of the effect over the background. The normal situation is that where R_e amounts to a few percent and the inequalities $R_e \leqslant R_p \leqslant R_\omega \leqslant R_b$ are satisfied, with R_p, R_ω, and R_b only slightly larger than R_e. As an illustration, in Fig. 8 we show a processed segment of the spectrum from Al_2O_3 measured at the DN-2 diffractometer.

High-resolution TOF diffractometers at operational neutron sources

In Table III we list all the high-resolution powder diffractometers in use at high-flux neutron sources. The last two are Fourier diffractometers. For comparison, we give the parameters of the DA diffractometer D2B (ILL, Grenoble), which is currently the best.

These characteristics should mostly be taken as guidelines, because the setups in question are constantly being improved and because the functional dependences are actually important and interesting. For example, the range of d_{hkl} is given only for the detector with the maximum resolution, while at nearly every diffractometer there are detectors at intermediate and small scattering angles which extend this interval.

Since there are very few of them, there are not enough high-resolution TOF diffractometers for experiments. For example, 276 applications were submitted for the HRPD in 1990, only 99 of which were granted. However, the introduction of new setups of this type in the next few years is not expected.

Examples of structure studies

The complexity of the structure problems which can be solved and the precision of the results obtained using the powder TOF diffractometer are mainly determined by the level of resolution attained. If the diffractometer resolution is $R \approx 0.01$, only the improvement of the atomic coordinates of structures which are not very complex can be considered. It is sometimes possible to improve the occu-

TABLE III. Parameters of high-resolution TOF diffractometers ($\Delta d/d \leqslant 0.003$) and the DA diffractometer D2B.

Parameters	GPPD IPNS	HRPD ISIS	NPD LANSCE	HRP KENS-1	Mini-SFINKS VVR-M	HRFD IBR-2	D2B HFR
L, m	20	96	32	16	6,5	20	—
d, Å	0,5–10	0,5–5	0,5–34	0,5–5	0,5–2,5	0,5–6	0,7–30
Φ_0, n/cm²/s	$2 \cdot 10^5$	$1 \cdot 10^6$	$1 \cdot 10^6$	$1 \cdot 10^5$	$1{,}2 \cdot 10^7$	$1 \cdot 10^7$	$1 \cdot 10^7$
V_s, cm³	5	2	5	5	5	2	5
R	0,0025	0,0005	0,0015	0,0030	0,0020	0,0005	0,0005

Note. The parameter R is given for the maximum scattering angle for $d=2$ Å, and for D2B it is given at the minimum of the resolution function. L is the distance from the source to the sample, d is the range of interplanar spacings, Φ_0 is the neutron flux at the sample, V_s is the "useful" volume of the sample, and $R=\Delta d/d$ is the diffractometer resolution.

pation factors or the isotropic thermal parameters of individual atoms. Resolution at the level $R \approx 0.003$ allows the occupation factors and the thermal parameters of the atoms to be improved independently, and in special cases the anisotropic thermal parameters can also be improved. Finally, if $R \leqslant 0.001$, both the complexity of the structure and the accuracy of the result become comparable to those in the case of experiments on single crystals and almost always significantly exceed the level of investigation of polycrystals using x-ray diffraction.

Experience with the structure analysis of diffraction data from polycrystals using the Rietveld method shows that if R changes weakly in a wide range of interplanar spacings, the number of peaks which can be included in the study is about $N_p = 1/3R$ for structures with an intermediate level of symmetry. Assuming that the number of peaks (essentially equivalent to the experimental points) exceeds the number of parameters to be improved by the required factor of five, we find that for $R = 0.001$ it is possible to simultaneously improve up to 70 parameters. These might include the occupation factors, the atomic coordinates, and the atomic thermal parameters. Naturally, in the course of analyzing the diffraction spectrum other characteristics of the crystal are also improved, for example, the lattice parameters, the determination of which at high-resolution diffractometers approachs a relative accuracy of 10^{-5}. The worth of the structure data extracted from a high-resolution TOF diffractometer can be evaluated from the following example.[32] The structure of benzene C_6D_6, space group Pbca, $a = 7.3551(3)$ Å, $b = 9.3712(4)$ Å, $c = 6.6994$ Å, $V = 461.75$ Å^3, was improved using the neutron diffraction pattern measured at the HRPD (Rutherford Appleton Laboratory). The measurement was made at $T = 4.2$ K for a sample of volume 5 cm^3 over a period of 9 hours. The segment of the spectrum in the range 0.606–1.778 Å consisting of 5382 points and containing 1040 peaks was processed. Eighteen position and 36 anisotropic thermal parameters were improved. The rms deviations of the relative coordinates were $(1-2) \times 10^{-4}$, which corresponds to errors in the C–C and C–D bond lengths of from 0.002 to 0.003 Å, which is altogether only three times worse than in the analysis of a single crystal of this compound.[33] In addition, the thermal factors, the determination of which is usually a stumbling block in the analysis of powder data, turned out to be in very good agreement with the values obtained in Ref. 33.

In principle, a powder diffractometer with $R \leqslant 0.001$ offers the possibility of determining the structure *ab initio*, as was demonstrated in Ref. 34 for the example of the previously unknown structure of $FeAsO_4$. The essence of this method is that for this resolution it is possible to measure a sufficient number of nonoverlapping peaks, so that direct methods can be used to determine the structure. The necessary steps for this are those well known in the structure analysis of single crystals, including the construction of the Patterson function. After solving the phase problem and determining the model of the structure, it is improved by the Rietveld method.

TOF diffractometers with average resolution are used

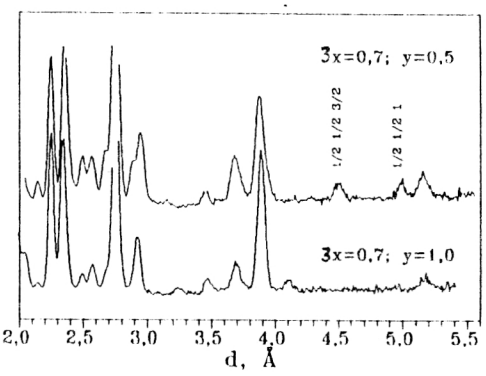

FIG. 9. Diffraction spectra of $YBa_2(Cu_{1-x}Fe_x)_3O_{6+y}$ measured at the DN-2 diffractometer at large d_{hkl}. After the oxygen was partially warmed peaks appeared corresponding to the antiferromagnetic structure with elementary cell doubled along all three axes.

to solve structure problems involving a small number of parameters or in experiments requiring additional conditions to be satisfied. For example, in a study of the system $YBa_2(Cu_{1-x}Fe_x)_3O_{6+y}$ using the DN-2 diffractometer,[35] the high luminosity at large d_{hkl} made it possible to find, in neutron diffraction patterns of samples with $x \geqslant 0.20$, weak auxiliary diffraction peaks (Fig. 9), a part of which is related to the appearance of a long-range antiferromagnetic ordering, i.e., the formation of a new elementary cell doubled along all three axes.

It is well known that in studying structures containing light atoms, primarily hydrides and oxides, it is neutron diffraction which offers the greatest possibilities. The accuracy with which the coordinates of light atoms can be fixed by neutron diffraction is much higher than in the case of x-ray structure analysis, including the analysis of single crystals. For example, the following numbers are quoted in Ref. 36 for oxides: 0.004, 0.011, and 0.050 Å; these are the average accuracies of determining the coordinates of oxygen atoms in a neutron powder experiment, in an x-ray study of a single crystal, and in an x-ray study of a powder, respectively. For hydrogen atoms the difference in the accuracy is even more striking.

In studies of the structure of high-temperature superconductors (HTSCs) the possibilities of neutron powder diffraction have been manifested especially clearly, first, owing to the absence of HTSC single crystals of good quality and, second, owing to the key role played by oxygen, which, because of the presence in HTSCs of heavy atoms like Ba, Bi, Y, and Cu, is practically invisible to x rays. It should be noted that TOF diffractometers have made a very important contribution in HTSC studies. Examples are the study of the temperature dependence of the $(La,Sr)_2CuO_4$ structure (HRPD, ISIS; Ref. 37), one of the first accurate determinations of the Y123 structure (SFINKS, VVR-M; Ref. 38), *in situ* experiments on the stoichiometry of oxygen in Y123 with heating in a controlled environment (SEPD, IPNS; Ref. 39), and the determination of the $Ba_{0.6}K_{0.4}BiO_4$ structure at low temperature (NPD, LANSCE; Ref. 40).

STUDIES OF SINGLE CRYSTALS USING TOF DIFFRACTOMETERS

The TOF diffractometer for single crystals

A technical feature of the modern single-crystal TOF diffractometer is the use of a one- or two-coordinate PSD. It is the position detector combined with wavelength sweeping of the diffraction spectrum that made it possible to drastically modernize the experimental scheme and realize the so-called "multidimensional diffractometry."[41,42] In fact, the multidimensionality reduces to the two- or three-dimensional case if a one- or two-coordinate PSD, respectively, is used. Here one coordinate is always the time of flight, and the sweep in it corresponds to scanning the reciprocal space of the crystal along the radius vector **H**. The other coordinates are the position groups of the detector, which in the reciprocal space corresponds to scanning in the plane perpendicular to **H**. Here there is parallel readout of information about the crystal in some volume of the reciprocal space without any rotations of the sample or detector. The size of the observed volume depends on the solid angle Ω_d of the detector and on the restrictions on the minimum and maximum values of the moduli of the vectors of the reciprocal space. The latter is related to the decrease of the neutron flux at large and small wavelengths. If the average Bragg angle θ_0 is not small, the observed volume (in the three-dimensional case) is

$$V^* \approx 2/3(\lambda_{\min}^{-3}-\lambda_{\max}^{-3})\sin^2\theta_0\Omega_d, \qquad (29)$$

where $\lambda_{\min}$ and $\lambda_{\max}$ are the boundaries of the working interval of the neutron spectrum. The number of sites of the reciprocal lattice contained in V^* depends weakly on the crystal orientation and is $n \approx V^* V_c$, where V_c is the volume of the elementary cell of the crystal. For $\lambda_{\min}=1$ Å, $\lambda_{\max} \gg \lambda_{\min}$, $\theta_0=45°$, and $\Omega_d=0.02$ the volume V^* is $\sim 10^{-2}$ Å^{-3}, and for crystals with average period of the elementary cell equal to 10 Å, 10 sites of the reciprocal lattice will be observed simultaneously.

The total number of simultaneously observable "elements" of the reciprocal space is considerably larger and is mainly determined by the detector resolution. The resolution of a modern two-coordinate PSD reaches 3 mm, and the total number of position elements is 10^3 or more. Since to each position element there corresponds a time spectrum, which can consist of several thousand channels, an internal memory of several million words is needed for the parallel recording of a complete set of data. In principle, present-day electronics allow this problem to be solved. However, this amount of data is often excessive and, depending on actual circumstances, it can be decreased considerably.

The problems which can be solved using single-crystal TOF diffractometers are conveniently divided into two classes: classical structure analysis, where the intensities of a large number of diffraction peaks are measured, and special experiments on analyzing the shape of the reciprocal-lattice sites.

Structure analysis using the TOF diffractometer

The idea behind the structure analysis of single crystals using the TOF diffractometer has the same essential features as the standard technique: the integrated intensities of a large number of diffraction peaks I_{int} are measured, the moduli of the structure factors are found in accordance with (5), their phases are somehow determined, and then the scattering density is constructed or the structure is improved by using the MNK. New features arise in the actual process of measuring I_{int} (as already mentioned) and in the appearance of great possibilities for solving the phase problem.

Structure studies involving single crystals at TOF diffractometers have developed somewhat more slowly than powder studies, although the first successful attempts were made 15 years ago.[43] In that study, carried out at the IBR-30 pulsed reactor (with average power 20 kW), a single crystal of deuteriumized lanthanum–magnesium nitrate $La_2Mg_3(NO_3)_{12}24D_2O$(LMN) (space group $R\bar{3}$, hexagonal lattice parameters $a=11.041$ Å, $c=34.610$ Å) was studied. Owing to the low intensity, a large sample of dimensions $5\times25\times25$ mm was used, which made it possible to measure 164 independent nonzero reflections. Improvement was done only for the coordinates and the isotropic thermal parameters of the deuterium atoms, and the x-ray data were used for the other atoms. The Zachariasen approximation was used to include extinction, and the effective spectrum was described by a parametric formula modeling the Maxwell distribution, taking into account absorption on the flight paths and the detector efficiency. In spite of the restricted amount of experimental data and the inclusion of the correction factors, which is considerably more complicated than in the case of the DA diffractometer, the data obtained turned out to be sufficiently accurate. For example, comparison with the results of the improvement of the hydrogen structure of LMN using the DA diffractometer[44] showed that the relative atomic coordinates coincide to within $(1-2)\times10^{-3}$.

The progress achieved in diffractometer luminosity during the last few years at pulsed sources can be judged from the results of Ref. 45, where modulation of the structure of Bi-2212 was studied on a crystal of dimensions $1.5\times1.0\times0.03$ mm, i.e., 7×10^4 times smaller in volume than the LMN crystal. In this study it was proved, first, that on the average the structure of $Bi_2(Sr,Ca)_3Cu_2O_{8+\gamma}$ can be described within the framework of the *Amaa* group with lattice parameters $a=5.397$ Å, $b=5.401$ Å, and $c=30.716$ Å. In addition, satellite reflections corresponding to the modulation vector $k=2\pi[\tau,0,1]$ with $\tau=0.213$, i.e., with modulation period 4.69 Å along the a direction, were discovered and measured. Improvement of the structure within the framework of the *Pnaa* group with elementary cell 19*abc* confirmed the reason proposed for the structure modulation: the penetration of one additional oxygen atom into the BiO layer, which leads to a noticeable modulation of the locations of the atoms also in other layers.

Of course, the success of this study was aided by the fact that the TOF diffractometer ensured continuous scan-

TABLE IV. Parameters of neutron resonances of nuclei which can be used to determine the phases of the structure factors (Ref. 16).

Isotope	E_0, eV	λ_0, Å	$2g\Gamma_{n0}$, meV	Γ, meV	b_0, 10^{-12} cm	b_i, 10^{-12} cm	b_i/b_0
^{113}Cd	0,178	0,678	0,968	115	0,68	4,6	6,8
^{149}Sm	0,098	0,915	0,6	61	0,79	7,2	9,1
^{155}Gd	0,027	1,747	0,13	108	0,81	1,7	2,1
^{157}Gd	0,031	1,614	0,59	106	0,81	7,1	8,8

Note. E_0 and λ_0 are the resonance energy and wavelength, g is the statistical factor of the resonance, Γ_{n0} and Γ are the neutron and total widths of the resonance, and b_0 and b_i are the potential and imaginary (for $\lambda=\lambda_0$) parts of the scattering amplitude (10^{-12} cm).

ning of large volumes of the reciprocal space. This feature is especially important for studying incommensurate modulated structures, when it is impossible to *a priori* predict both the proper coordinates of the satellite peaks and their changes in the course of a phase transition or under the influence of an external field. The authors of Refs. 46 and 47, in experiments carried out at the DN-2 TOF diffractometer, obtained extensive information on the modulation of the structure of a ferroelectric with diffuse phase transition $Sr_xBa_{1-x}Nb_2O_6$ for a wide range of temperatures, external electric field, and composition variation.

As shown above, the efficiency of the measurement of reflections from a single crystal using a TOF diffractometer with a two-coordinate PSD grows in proportion to the volume of an elementary cell of the crystal. It should therefore be expected that an important structure problem for single-crystal TOF diffractometers may be the analysis of organic and biological crystals with large V_c. The first neutron-diffraction study of the structure of the protein crystal myoglobin was carried out in 1968 at the Brookhaven reactor.[48] Similar experiments were carried out for the trypsin and lysozyme crystals in the 1970s, but were not very common, mainly owing to the great difficulty in carrying them out using the DA diffractometer. In fact, the pure time to measure the 10^4 reflections from the myoglobin crystal needed to construct the Fourier synthesis with a resolution of 2 Å was about 10^3 hours, which lies at the limit of the reasonable duration of an experiment. Simple estimates show that this time can be decreased by at least a factor of 10 when a modern TOF diffractometer is used.

An interesting consequence of the increased volume of the elementary cell of a crystal is the rapid decrease of the effect of extinction on the measured intensities, which eliminates one of the main problems in structure analysis based on the TOF diffractometer. This effect is related to the decrease on the average of the structure factors of the crystal as the structure becomes more complicated. It can be estimated quantitatively as follows.[49] The fraction of reflections having $|F|^2$ larger than some given value z satisfies the equation

$$n(z)=\exp(-z/\overline{|F|^2}), \qquad (30)$$

where $\overline{|F|^2}=\Sigma b_i^2=N\overline{b^2}$, N is the number of atoms in a cell, and b_i is the coherent scattering length of the ith atom. Using Eq. (14) to estimate the extinction coefficient (the Zachariasen approximation, a type-I crystal), for the crystal, it is possible to calculate the number of peaks for which the extinction will be larger than a given amount. In the case of the myoglobin crystal used in Ref. 48 ($\overline{b^2}=0.38\times10^{-24}$ cm^2, $T=0.27$ cm), the extinction will be noticeable only for 750 of the 10 000 measured peaks, $y\leqslant0.99$, and it will be important for only 40, $y\leqslant0.85$.

Another attractive feature of using the TOF diffractometer for structure studies of complex crystals is the possibility of solving, independently of x-ray structure analysis, the problem of determining the phases of the structure factors using resonance neutron scattering.[50] Four stable isotopes are known which have resonances at energies suitable for diffraction experiments (Table IV). The successful use of resonance scattering depends on how large is the intensity difference (the Baywoot difference) for inverse reflections (hkl) and $(\overline{hkl})$, which is determined by b_i/b_0. When x-ray anomalous scattering is used, this ratio is usually less than 0.1–0.2. We see from Table IV that in the case of neutrons it is much larger, so that it is possible to consider only relatively low concentrations of resonance nuclei in the structure, for example, using ^{113}Cd it is possible to analyze a structure containing 1 atom per 2000 atoms.[51] The usual method of using resonance scattering to determine the phases of the structure factors is the combined analysis of sets of data measured at two (sometimes three) wavelengths. Here the largest Baywoot differences are observed if λ_1 and λ_2 are chosen such that $|b_0+b_i(\lambda_1)|=|b_0+b_i(\lambda_2)|$ to the left and right of the resonance. The TOF diffractometer is obviously much better suited for realizing this program than the DA diffractometer: there is no problem with exchange and the choice of the needed wavelength, the neutron flux for $\lambda\leqslant1$ Å is considerably higher, and, finally, the resolution at small wavelengths is also much better in the TOF diffractometer.

Data compression in experiments on single crystals

The amount of recorded information can be decreased significantly in a structure experiment on a single crystal

using a TOF diffractometer. This is related to the fact that the standard realization of the diffraction-data acquisition process with constant scanning step in the wavelength (the channel width of the time analyzer) and in the angular variables (the width of the position group of the detector) leads to an excessive amount of recorded information. For example, when a two-coordinate PSD with 1024 cells (32 by 32 in each coordinate) is used, the recording of the time spectra in a range of 10 Å requires an internal memory of about 4×10^6 words. The idea behind data compression is that only the values of the integrated intensities of the diffraction peaks, not the complete measured distribution $I(\mathbf{Q})$, are needed for the structure analysis. For separating the background and analyzing partially overlapping peaks it is sufficient to have 4–6 points on each side of the parallelepiped in which the peak is inscribed. Here the recording of even 100 peaks requires no more than 21 600 storage registers, i.e., the realization of diffraction-spectrum acquisition in some modified coordinate system would lead to a large decrease in the amount of recorded data. The choice of coordinate system for this is to a certain degree arbitrary. Arguments can be given in favor of the following two variants:

the directions in which the Q space is divided coincide with the directions of the elementary translations in the reciprocal lattice of the crystal;

one of the vectors of the new coordinate system is parallel to the vector $\mathbf{Q}_0$ (directed, for example, toward the center of the detector), and the other two are perpendicular to it. The most symmetric filling of the reciprocal space by the subdivision cells is obtained in the first variant because the reciprocal elementary cell and the subdivision cell have the same shape. The most economical covering of the observed volume of the reciprocal space by the subdivision cells is obtained in the second variant and, in addition, the orientation of the Q-space subdivision mesh is independent of the orientation of the crystal. In any case, two operations must be carried out during the acquisition stage:

transformation from the coordinates x,y,t (where x and y are the coordinates of the point where the neutron is recorded in the detector and t is the time of flight) to the coordinates in the $\mathbf{Q}$ space;

association of a detection event with some cell in Q space, i.e., increase of its content by unity. An algorithm suitable for this was published in Ref. 52, but has not been fully realized in practice.

A simpler method of data compression which has already been realized[53] is that of using special time encoders with channel width increasing with time. This idea originates from the fact that in recording the diffraction pattern from the Bragg plane of a single crystal, one observes reflection orders located at points $t_n=t_1/n$ on the time axis, where t_1 is the time of flight for the first-order reflection and n is the order number. If the channel width of the time encoder used to form the time scale is constant, the filling of the analyzer memory with useful information will be very nonuniform, because the distance between adjacent reflection orders varies as t_n^2. It is easily seen that if the width of the time channel grew as t^2, the diffraction orders of the reflection would be equidistant from each other. Actually, $\Delta H\sim\Delta k\sim\Delta t/t^2$, where H is the modulus of the reciprocal-lattice vector, k is the modulus of the neutron wave vector, and $\Delta H=\text{const}$ if $\Delta t\sim t^2$, as required, because the reflection orders are equidistant from each other on the H scale: $H_n=nH_1$.

The relation between the number of the time channel and the neutron time of flight, if the channel width varies as $\tau(t)=t^2/\beta$, can be obtained from the differential relation $dN(t)=dt/\tau(t)$, from which it follows that

$$N(t)=\int_{t_0}^{t} dt/\tau(t)=\beta(1/t_0-1/t)$$
$$=M_{\max}(1-t_0/t), \tag{31}$$

where t_0 is the time at the start of the recording and $M_{\max}=\beta/t_0$ is the maximum channel number. If $t\gg t_0$, the compression coefficient, i.e., the decrease of the needed number of channels compared with the case $\tau=\text{const}$, is $t_{\max}/t_0$ and is equal to n when all reflection orders from the first to the nth are recorded.

When this data-compression method is used, it is necessary to take into account certain factors. First, the peaks are distorted and their maxima (and centers of mass) are shifted. Second, since the channel width becomes a rapidly growing function of the channel number,

$$\tau(N)=\tau_0/(1-N/N_{\max})^2, \tag{32}$$

functions which are quasiconstant in the time of flight (for example, the detector background) are transformed into growing ones in accordance with Eq. (32). The width of the diffraction peaks never grows more rapidly than t, so that in some cases a linear increase of the width of the time channel $\sim t$ may be optimal.

Analysis of the shape of the reciprocal-lattice sites

The need to analyze the shape of the reciprocal-lattice sites of a crystal arises in many problems which can be solved using single crystals. Here we shall discuss only an experiment involving a ferroelastic crystal undergoing a phase transition to a phase of low symmetry. It is well known that such a transition is accompanied by the splitting of the crystal into domains—transformation twins, which also leads to a change of shape (splitting) of the Bragg peaks.

The shape of a single diffraction peak is given by Eq. (1), and to isolate the contribution of the crystal itself it is necessary to know the resolution function and perform the deconvolution of $I(\mathbf{Q}_0)$. However, if the width of the resolution function is small compared with the splitting of the peaks in the phase transition (which, incidentally, is a necessary condition for the experiment to be successful), it is usually sufficient to include only the main factors determining R and to use the Gaussian approximation. In this approximation it is convenient to combine the mosaic structure of the crystal with the resolution function. Then the diffraction peak is an ellipsoid in Q space with dimen-

sions and orientation determined by the dispersions of the distributions which are included.

For example, in the two-dimensional variant (scanning in the time of flight using a one-coordinate PSD) the shape of the peak is[54]

$$I(\xi,\gamma)=I_0\exp(-A\xi^2-2B\xi\gamma-C\gamma^2), \qquad (33)$$

where $\xi=(k-k_0)/k_0$ is the relative deviation of the modulus of the neutron wave vector from the nominal value, $\gamma=2(\theta-\theta_0)$ is the deviation of the Bragg angle from the nominal value, and A, B, and C are quantities depending on the dispersions of the principal distribution functions affecting the shape of the peak, namely, the angular distribution of the neutrons in the primary beam, the distribution of the orientations of the mosaic blocks, and the time-of-flight distribution of the neutrons from the source.

The formation of a domain structure in a ferroelastic crystal leads to splitting of the peaks (formation of a compound reciprocal lattice; Ref. 55). The resulting distribution can be represented as the sum of several functions $I(\xi,\gamma)$ with shifts along the ξ and γ axes:

$$I_s(\xi,\gamma)=\sum r_i I(\xi-\xi_i,\gamma-\gamma_i), \qquad (34)$$

where r_i are the weights and (ξ_i,γ_i) is the position of the ith component. The positions of the components found experimentally can be related to the coordinates of the corresponding points in the reciprocal space of the crystal, i.e., the spontaneous shear angle, the changes of the linear dimensions of the elementary cell, and so on, can be determined. The volume of the reciprocal space in which I_s is distributed is usually easily observed using a TOF diffractometer with a PSD. Since the entire distribution (34) is measured in parallel, there is obviously an enormous saving in time compared with point scanning if it is recalled that the number of points which are measured reaches several thousands. In addition, an important factor is the unvarying orientation of the crystal during the exposure, which greatly simplifies the data analysis.

Let us see how these considerations have been used to analyze the domain structure of the ferroelectric–ferroelastic crystal KD_2PO_4 using a TOF diffractometer at the IBR-30 pulsed reactor at the JINR Nuclear Physics Laboratory.[56]

Crystals of potassium dideuterium phosphate at room temperature in the paraphase have a tetragonal cell (space group $I\bar{4}2d$) with parameters $a=7.468$ Å and $c=6.979$ Å. In the phase transition ($T_c\approx214$ K for 92% deuterium content) the symmetry is lowered to rhombic symmetry and $\Delta a=-\Delta b\approx0.055$ Å. It is sometimes more convenient to represent this transition as the appearance of a monoclinic cell owing to a pure shear along the diagonals of the square (a,b). In this case the transition parameter is the spontaneous-shear angle u_{xy}. In fact, owing to the need to conserve the continuity of the crystal, the transition cannot be realized by the mechanism of a pure shear. Instead, simple shifts of the lattice in directions of the type [100] occur which, in principle, can be treated as a pure shear in the [110] direction followed by rotations of the resulting

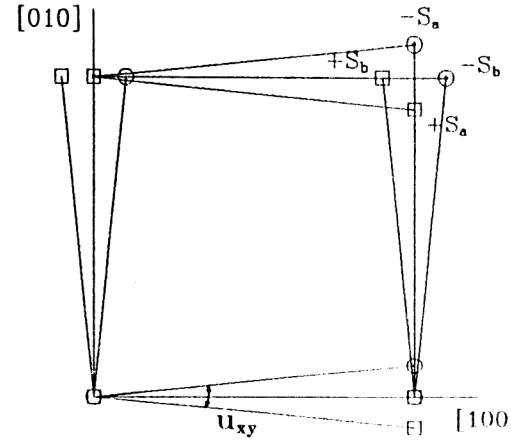

FIG. 10. Schematic diagram of the splitting of the reciprocal-lattice sites of DKDP upon twinning as a result of simple shears in the [100] and [010] directions. For the site [$hh0$] we show the points corresponding to two types of domain (S_a and S_b) and two signs of the polarization; u_{xy} is twice the spontaneous-shear angle.

rhombi (Fig. 10). In this case reflections of the [$h00$] type must be split into three components, and any other reflections must be split into four components. The distributions shown in Fig. 11 confirm this. The size of the splitting can easily be used to calculate the spontaneous-shear angle (for DKDP it is 31.3′) or the changes of the cell parameters in the transition, and the intensity of the individual components of the split site characterizes the relative number of domains with a particular orientation. It is the latter question which is usually analyzed if the crystal is subjected to an external field. In Fig. 12 we show how the picture is changed in one of the sites of the DKDP lattice when the strength of the electric field imposed on the crystal is increased. We see that the crystal polarization process (monodomainization) consists of several stages. First the number of domains with polarization opposite to the applied field is decreased, and then the number of domains of one of the two types S_a or S_b, whichever is for some reason

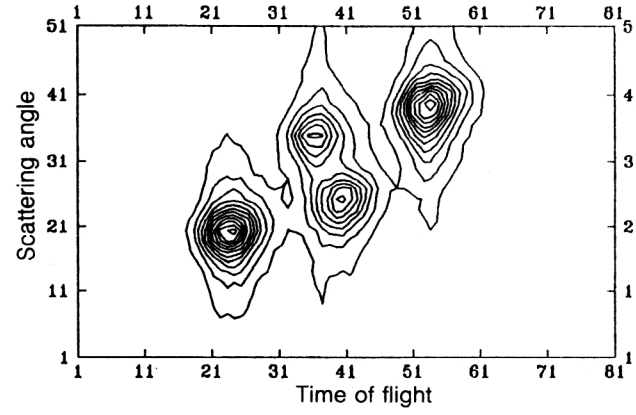

FIG. 11. Intensity distributions at the site (440) of the DKDP crystal in the low-symmetry phase ($T=80$ K), shown in the form of a contour plot. The time of flight is on the horizontal axis, and the scattering angle is on the vertical axis (both in conventional units).

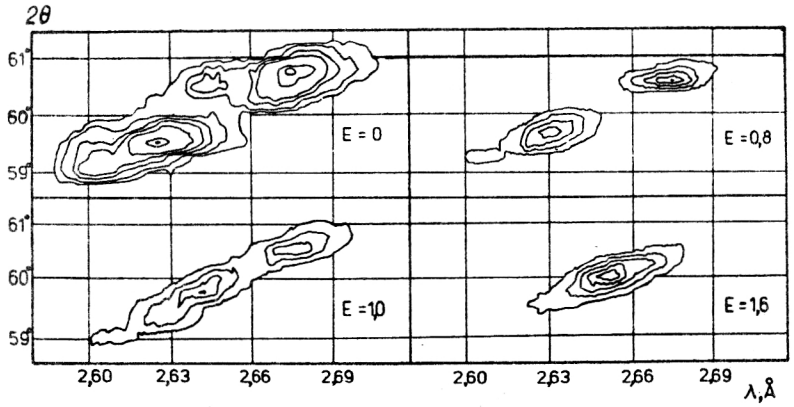

FIG. 12. Variations of the intensity distribution at one of the reciprocal-lattice sites of DKDP for $T=210$ K as the electric field strength at the crystal is increased: $E=0$, 0.8, 1.0, and 1.6 kV/cm.

energetically less favorable, begins to decrease. Simultaneously or after a small delay the $+S_a$ and $+S_b$ sites begin to move toward each other, so that the final state corresponds to the rotation of the elementary cells to the position of a pure shear from the initial paraelectric state.

Further experiments using DKDP crystals have shown[57] that the nature of the polarization and repolarization processes depends on the value of the coercive field of the crystal, i.e., on its real structure, but the stage of a polydomain state practically always arises in the repolarization of the crystal.

Processes of the polarization type in pure ferroelastic crystals in the presence of an external pressure or the temperature dependence of the transition parameter can be studied in a similar manner. For example, in Fig. 13 we show the temperature dependence of the spontaneous-shear angle found[58] from analysis of the splitting of the (002) site of the ferroelastic $KD_3(SeO_3)_2$.

An example of how the observation of the number of components of a site and the form of the splitting helps to establish the symmetry of the ferroelastic phase can be found in Ref. 59, where the crystal $LiKSO_4$ was studied. In Ref. 60 it was necessary to analyze the shape of the reciprocal-lattice sites in studying diffuse scattering from the crystal $Na_{0.5}Bi_{0.5}TiO_3$ (NBT). A peak was found in the diffuse scattering in the [001] direction, indicating the presence of lattice modulation along the z axis. Analysis showed that the modulation is related to correlated rotations of the oxygen octahedra in layers perpendicular to the z axis, with competition between the parallel and antiparallel rotations of the octahedrons.

Analysis of long-period structures

Let us consider some features of the analysis of neutron diffraction patterns from long-period structures such as multilayers from lipid membranes. It was shown in Ref. 6 that studies of such structures using the TOF diffractometer are very effective, but the usual methods of extracting the structure factors from the measured intensity distributions can prove inapplicable. Actually, the range of wavelengths in which diffraction reflection is observed is $\Delta\lambda=2d\Delta\theta\cos\theta_0$, and for large d, small θ_0, and large-scale mosaic structure of the sample, as frequently occurs precisely for long-period structures, $\Delta\lambda$ can reach 1 Å and more. In this case special analysis taking into account the resolution function is required to transform from the intensities of the diffraction peaks to the structure factors.

The starting point for the analysis is Eq. (1), which describes the three-dimensional intensity distribution at a reciprocal-lattice site. However, the problem simplifies drastically if we assume that it is possible to factorize the resolution function in the form

$$R(Q)=R_1(Q_x,Q_y)R_2(Q_z), \tag{35}$$

where R_1 and R_2 are functions determining the resolution in the horizontal and vertical planes, respectively. As shown in Ref. 62, this is valid for a sample of sufficiently small dimensions and for scattering angles which are not too small. If in the TOF diffractometer two-dimensional scanning is performed using a one-coordinate PSD, the integration over the variable Q_z (the vertical aperature of the detector) is done automatically and the measured intensity is determined by

$$\sigma(Q_x,Q_y)=\int R_2(Q_z)\sigma(\mathbf{Q})dQ_z, \tag{36}$$

which for sufficiently large width R_2 is proportional to the projection of the scattering cross section on the horizontal plane. In the Gaussian approximation for the distribution functions the dispersion of R_2 is

$$D_2=Q_0^2[D_\delta+D_\omega/L_2^2]/(4\sin^2\theta_0), \tag{37}$$

where D_δ is the angular dispersion of the primary neutron beam in the vertical plane, D_ω is the detector contribution, $D_\omega\approx\omega^2/12$, ω is the vertical dimension of the detector, and L_2 is the distance from the sample to the detector. The smearing of $\sigma(\mathbf{Q})$ in the vertical plane is usually completely determined by the mosaic structure of the sample η and, accordingly, the condition for complete projection of $\sigma(\mathbf{Q})$ on the horizontal plane is the inequality $\eta^2\ll D_2$. The total dispersion of the scattered beam in the vertical plane is $D_v=\eta^2+D_2$, and the factorization (35) is meaningful if $\theta_0\gg D_v$. For actual samples of lipid membranes θ_0 should be at least a few degrees. In this case the two-dimensional profile of the diffraction peak can be represented as (33), where I_0 has the form

$$I_0=\Phi(\lambda)\lambda^3|F|^2/(V_c^2\sin 2\theta)A(\lambda,\theta), \tag{38}$$

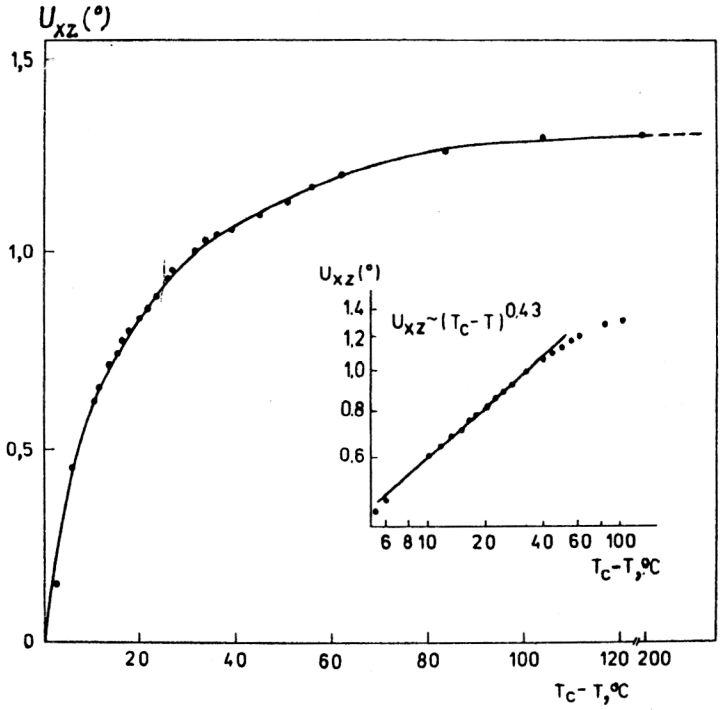

FIG. 13. Temperature dependence of the spontaneous-shear angle of the ferroelastic crystal $KD_3(SeO_3)_2$ found by analyzing the site splitting as the sample is cooled. On the doubly logarithmic scale (inset) it can be seen that the classical dependence of u_{xz} on $T_c - T$ with exponent 0.43 holds.

where, as before, Φ is the effective neutron spectrum, A is the absorption factor, and I_0 must be integrated over λ and θ.

The question arising at this stage is whether or not it is possible to integrate over both variables or at least only over θ before normalization to $\Phi(\lambda)$ and the inclusion of absorption. It follows from analysis that this is possible if the dispersion of the primary beam, which in general depends on λ, remains much smaller than the doubled mosaic structure of the sample. Experiments with lipid multilayers carried out using the DN-2 diffractometer[63] showed that this condition is usually satisfied for all the reflection orders except the first. In Fig. 14 we see how the structure factors of the diffraction peaks from a multilayer of egg lecithin depend on the ratio of H_2O and D_2O in the sample.[64] The linearity of these dependences indicates that the corrections display the correct behavior in going from the intensities to the structure factors.

4. THE STUDY OF IRREVERSIBLE TRANSIENT PROCESSES

Despite the relatively small value of the neutron flux from existing sources, the specific features of neutron diffraction make it an extremely powerful tool for studying transient processes in condensed media. Systematic experiments of this type were begun only recently, but it can already be stated that a new branch of neutron diffraction has been founded: real-time neutron diffraction (RTND), understood as the observation by means of neutron scattering of rearrangement of the structure of matter at the atomic level directly during this process. In general there is both diffraction of the neutrons and small-angle or diffuse scattering of them, although in most experiments only the diffraction spectra are recorded, as they are the most intense component of the scattering process. Compared with x-ray or synchrotron radiation diffraction, which are also widely used to observe transient processes, RTND has all the advantages of neutrons, primarily the ability to "see" light atoms near heavy ones and to distinguish isotopes of elements. Often, in experiments carried out in real time an important factor is the high penetrating ability of neutrons.

The scale of the characteristic times accessible to study varies considerably, depending on whether the process is reproducible or not. For reproducible phenomena it is possible to reach time scales of order 10^{-3} s, as in the polarization reversal of the $NaNO_2$ crystal,[65] and even 10^{-4} s, as in the case of the spin-flop transition in a pulsed magnetic field in the Cr_2O_3 crystal.[66] In these experiments the lower

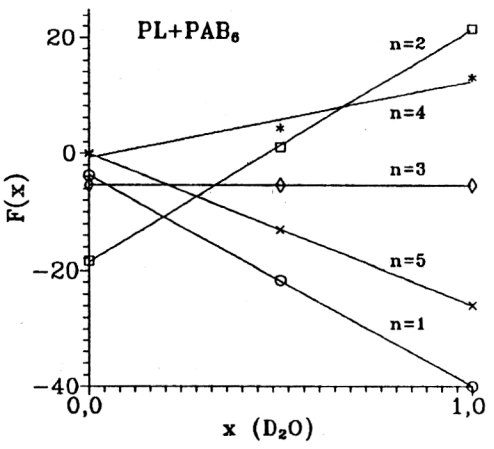

FIG. 14. Dependence of the structure factors on the D_2O content for a sample from the total lipid fraction of egg yolk (PL) with implanted molecules of diester hexylphosphorous acid (PAB_6). The linear dependence of $F(x)$ is well satisfied for all reflection orders. Measurements of $F(x)$ were carried out for the three values $x=0$, 0.5, and 1.

TABLE V. Parameters of high-luminosity TOF diffractometers and the DA diffractometer D1B used for real-time studies. The DPP diffractometer is under construction.

Parameters	SEPD, IPNS	HID, LANSCE	DN-2, IBR-2	DPP, IBR-2	D1B, HFR
L, m	14	12	24	28	—
d, Å	0,5–30	0,5–30	0,8–30	0,8–30	1,5–10
Φ_0, n/cm^2/s	$2\cdot10^5$	$1\cdot10^6$	$1\cdot10^7$	$5\cdot10^7$	$2\cdot10^6$
V_s, cm^3	5	5	5	5	1
Ω_d, sr	0,1	0,1	0,02	0,08	0,1
R	0,005	0,005	0,01	0,01	0,01
J	$1\cdot10^5$	$5\cdot10^5$	$1\cdot10^6$	$2\cdot10^7$	$2\cdot10^5$

Note. The notation is as in Table III; Ω_d is the solid angle of the detector system, and $J=\Phi_0 V_s \Omega_d$ is the diffractometer luminosity.

bound on the time resolution arises mainly owing to the uncertainties in the action of the reversal pulses on the crystal. The statistical accuracy of the measured spectra depends on the number of repetitions of the process and can be very high.

In the case of an irreversible process, for example, a chemical reaction, its observability is determined by the condition $t_s \ll \tau$, where τ is the characteristic time for the process and t_s is the time for the measurement of a single spectrum with a level of statistics sufficient for the goals of the experiment. The quantity t_s depends on the neutron flux in the primary beam and on the area and scattering capability of the sample, and for the neutron diffractometers of highest luminosity at stationary reactors it is 5–15 min (D1B at the HFR reactor at ILL, Grenoble,[67] DISK at the IR-8 reactor at the Kurchatov Institute, Moscow[68]). At several pulsed neutron sources (ISIS, LANSCE) roughly the same times are obtained as at the IBR-2 reactor, which has a record pulsed flux, and experiments with $t_s \leqslant 1$ min are performed. Later we shall discuss the experimental setup and examples of the use of the TOF diffractometer for studying irreversible transient processes, which are referred to as RT (Real-Time) experiments.

A TOF diffractometer with high luminosity

Let us consider the factors affecting the luminosity of the TOF diffractometer. The number of neutrons recorded per unit time can be estimated using the following expression:

$$I=\Phi_0 S \frac{\Omega_d}{4\pi}\delta, \tag{39}$$

where S is the sample area and δ is its scattering capability. The neutron fluxes obtained range from 10^5 (SEPD, ANL) to 10^7 neutrons/cm^2/s (DN-2, JINR), and the solid angle of the detector systems ranges from 0.04 to 0.1 sr. For a sample area of 5 cm^2 and scattering capability of $\delta \approx 0.1$ we find that the total counting rate can reach 5×10^5 neutrons/s. This is very high, enough to ensure measurements with a time resolution on the order of minutes and even seconds, and the question is how useful are the recorded neutrons, i.e., what is the information content of the measured diffraction spectrum. This factor is primarily related to how large (or sufficient) is the range of d_{hkl} which can be simultaneously recorded and what is the diffractometer resolution. As is well known, under these conditions the diffractometer can be optimized either in the luminosity or in the resolution, so that losses in the resolution are unavoidable in the construction of TOF diffractometers with high luminosity. However, it turns out that for a large class of transient processes which are very well suited to neutron-diffraction study, such as chemical reactions in the solid phase, hydration and dehydration of biomolecules, isotope exchange in matter (and many others), an easily attainable level of resolution is $\Delta d/d = 0.005$–0.01. This allows the use of relatively short (10–15 m) path lengths and moderate angular collimation of the primary and scattered beams. It is precisely for this reason that the high-luminosity diffractometers mentioned above were constructed. The characteristics of some TOF diffractometers used to carry out RT experiments are given in Table V.

Examples of RT experiments

Let us consider several examples of experiments carried out in real time. They are most often performed by varying some external parameter, for example, the temperature. In this case the time and temperature axes coincide, continuous diffraction tracking of the temperature changes of the structure is performed, and the experiment is referred to as a thermodiffraction experiment. If the tracking of the structure of the temperature changes is done considerably more rapidly than the measurement of the diffraction spectra, the time resolution of the observation of the structure changes is completely determined by t_s, the time to accumulate the required statistics. In this regime it is convenient to observe phase transformations in the system as a result of structure phase transitions or chemical reactions. The regime of jump-like changes of the external conditions is used to study the kinetics of processes and to determine the characteristic constants (the relaxation time, the activation energy, and so on).

It should be noted that if a structural transformation process is studied and the neutron-diffraction patterns are analyzed using the Rietveld method, the accuracy of the

TABLE VI. Structure parameters of $YBa_2Cu_3O_{6+\delta}$ determined from data obtained using the DN-2 (t_s=5 min) and SEPD (t_s=2 h) diffractometers.

Parameters	T = 940° C, DN-2	T = 818° C, SEPD
a, Å	3,915(1)	3,9018(1)
c, Å	11,966(3)	11,9403(5)
z(Ba)	0,1916(7)	0,1914(3)
z(Cu2)	0,360(1)	0,3590(3)
z(01)	0,152(1)	0,1508(5)
z(02)	0,379(1)	0,3792(2)
z(04)	0,152(1)	0,1508(5)
δ	0,12(2)	0,42(3)
R_{wp}	0,0447	0,0743
R_{exp}	0,0458	0,0497

Note. The numbers in parentheses are the statistical error in the last significant figure. The improved DN-2 data were obtained for fixed thermal factors of the atoms.

structure parameters obtained depends both on the statistics collected, i.e., on t_s, and on the resolution of the diffractometer at which the experiment is carried out. As an example, in Table VI we give the data on the analysis of the structure of $YBa_2Cu_3O_{6+\delta}$ at high temperature before the start of the cooling process, during which the structure is enriched by oxygen. The spectra measured at the DN-2 diffractometer, which has high luminosity and average ($\sim$1%) resolution, and the SEPD diffractometer, which has significantly lower luminosity but resolution 3–4 times better, were analyzed. The expected R factors (R_e) characterizing the level of the accumulated statistics turned out to be roughly equal (the measurement time at the DN-2 was 25 times smaller), and the rms deviations of the parameters were 2–5 times smaller at the SEPD, exclusively owing to the better resolution.

A. Chemical reactions

A resolution at the 1% level is quite adequate in many cases for analyzing chemical transformations during a reaction in the solid phase, and the features of prime importance for estimating the observability of the process are the diffractometer luminosity and the range of simultaneously observable d_{hkl}. In the case of simple reactions with a small number of intermediate phases it is sufficient to follow the time evolution of several diffraction peaks measured at fixed scattering angle. For example, in Fig. 15 we show a sequence of spectra measured with t_s=5 min in the course of the oxidation of metallic copper in air. The evolution of the diffraction peaks belonging to the initial phase (Cu), the intermediate phase (Cu_2O), and the final phase is clearly visible. The relative changes of the intensity of the diffraction peaks characterize the content of the corresponding phase. A considerably more complicated analysis is necessary in the RT experiment on the synthesis of the compound $YBa_2Cu_3O_x$ from the initial components Y_2O_3, $BaCO_3$, and CuO in air.[69] The neutron-diffraction patterns were measured at several scattering angles over 6 hours with t_s=5 min as the temperature was varied from room temperature to 940 °C. The result of their analysis is shown in Fig. 16 in the form of dependences of the intensities of diffraction peaks belonging to the individual phases. A more accurate quantitative analysis of the content of the various phases in the sample can be made using the Rietveld method,[70] which also gives a good explanation of the dependences of the structure parameters on the time or temperature (Fig. 17).

B. Isotope exchange

The dependence of the scattering probability on the isotope content of the medium is one of the most important features of the interaction of neutrons with matter. This is manifested especially clearly in interactions with hydrogen and deuterium: the coherent scattering lengths for these

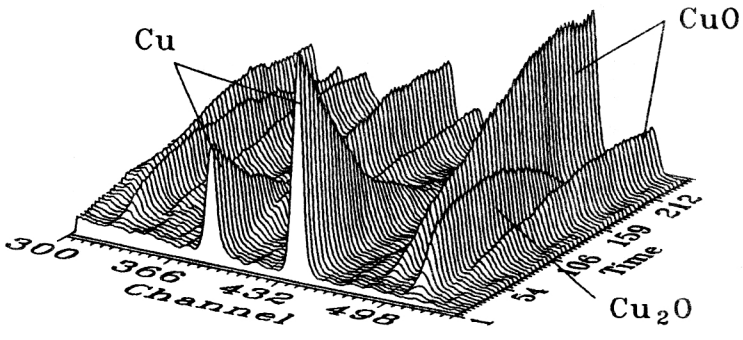

FIG. 15. Time evolution of the diffraction spectra measured during the reaction $2Cu+O_2 \rightarrow 2CuO$. The time axis is also the temperature axis and ranges from 250 °C to 650 °C (the beginning and end of the scale, respectively). About 50 diffraction spectra, each measured for 20 s, are located along the time axis.

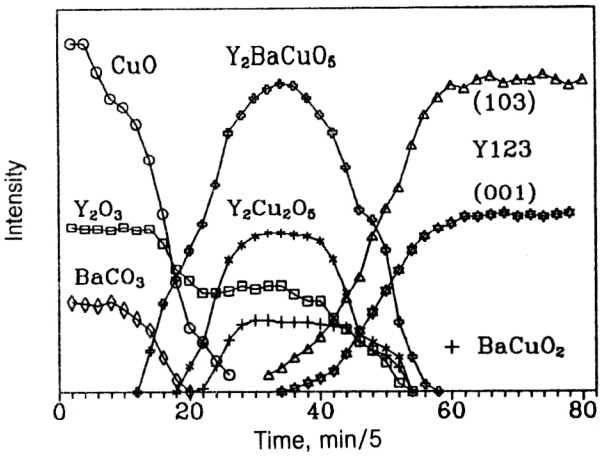

FIG. 16. Time variation of the intensities of several diffraction peaks belonging to different compounds during the chemical reaction producing $YBa_2Cu_3O_{6+y}$. The relative intensity of the peaks characterizes the content of the phase in the reacting mixture.

isotopes, b_H and b_D, are, respectively, -0.374 and 0.665 in units of 10^{-12} cm. Examples of kinetic experiments based on the large difference between b_H and b_D are observations of the replacement of H_2O by D_2O and vice versa in collagen, myelin, and multilamellar lipid structures. In particular, in Ref. 71, in an experiment carried out using the DN-2, it was shown that the process of substitution with simultaneous change of the moisture content is complex, i.e., it consists of several stages with different time constants. It was impossible to observe the first, most rapid stage in these experiments; it was only estimated that its time constant is about 1 min. The next two stages occurred with time constants of 3–4 min and 10–30 min. Their actual value depended on the initial and final moisture contents. The problem of observing the initial stage of the process was formulated and solved in Ref. 72.

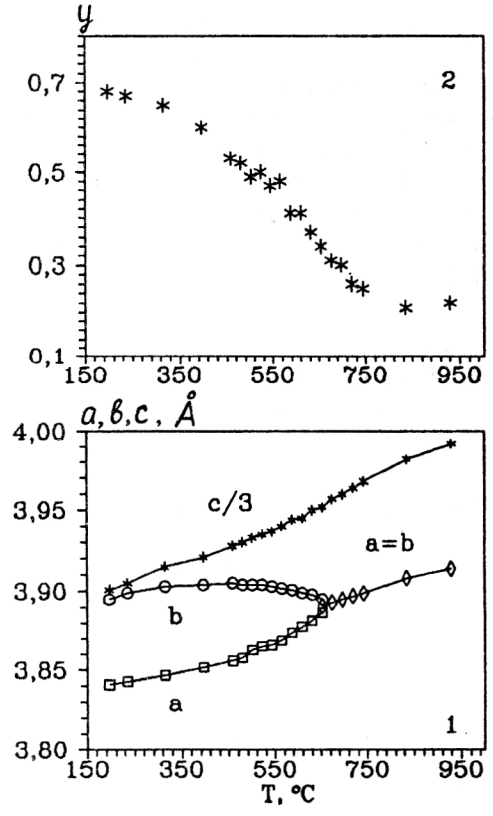

FIG. 17. Changes of the tetragonal phase of $YBa_2Cu_3O_{6+y}$ during cooling from 940 °C to 160 °C: (1) parameters of the elementary cell (in Å) (for $T \approx 660$ °C the structure becomes rhombic); (2) total oxygen content y in Cu–O chains.

A sample in the form of oriented layers of phosphatidylcholine–phosphatidylglycerin (PC:PG, stoichiometry 1:1) deposited on a cover glass (24×24 mm) was placed in a sealed chamber with windows of aluminum foil. The moisture content in the chamber was specified by placing in it a cuvette with a cloth moistened with heavy or light water. The replacement of one cuvette by another took place during 1 s without communication with the external medium.

It can be assumed that the change of the amount of D_2O in the sample in the replacement process $H_2O \rightarrow D_2O$ (or of H_2O in the reverse process) will follow an exponential law, i.e.,

$$m(t) = M(1 - e^{-t/\tau}), \tag{40}$$

where t is the time from the start of the process, M corresponds to the mass of the water in the saturated state, and τ is the characteristic time. Since the total structure factor of the lipid bilayer can be represented as the sum $F_T = F_L + F_W$, where F_L and F_W are the structure factors of the lipid and water parts and $F_W \sim m(t)$, the time dependence of F_T must also be exponential: $F_T(t) = F_\infty + F_1 e^{-t/\tau}$, where F_∞ and F_1 are constants. In the absence of extinction effects $F_T \sim I^{1/2}$, where I is the peak intensity, and, accordingly, the dependence $\ln|F(t) - F_\infty|$ must be linear in time. This function is shown for the two processes in Fig. 18, where it is clear that the linearity does actually occur. The quantities $\tau(H \rightarrow D)$ and $\tau(D \rightarrow H)$ are determined from the slope of the lines and are 92 and 71 s, respectively.

C. A phase transition

Let us see how information can be obtained in the observation of processes occurring in the warming of heavy ice D_2O from liquid nitrogen temperatures to room temperature.[73]

Earlier it was already known that, in addition to crystalline modifications, in ice it is possible to have two amorphous phases (*lda* and *hda*) differing in density, which are obtained from hexagonal ice *Ih* at high pressure. Another possible way of obtaining amorphous ice from the hard high-pressure phase VIII was discovered in Ref. 74. In that study the sequence of transitions VIII → *lda* → *Ic* → *Ih* was observed, where *Ic* is the cubic phase. It was suggested that the low-density amorphous phase *lda* is formed from the high-density phase *hda*, but it was not possible to observe this process experimentally.

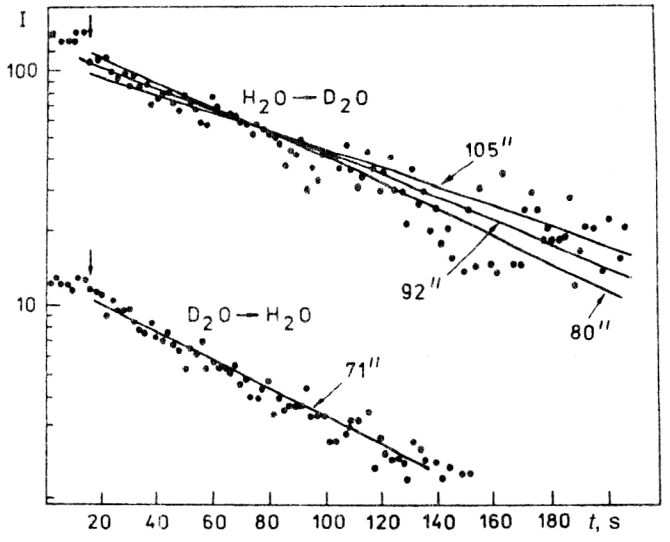

FIG. 18. Time dependences $\ln|F(t)-F_\infty|$ for D_2O substitution by H_2O and vice versa. The lines (drawn by hand) correspond to different characteristic times of the exchange process.

In Ref. 73 transitions of heavy ice from the hard phase VIII upon heating from 94 to 290 K were observed in real time with a resolution of 5 min for the purpose of finding the VIII→*hda* phase transition. A sample (99% D_2O) of weight 0.3 g at room temperature was compressed up to 2.6 GPa, held there for one hour for equilibrium to be established, and cooled to 100 K, after which the pressure was lowered to atmospheric pressure. Then the sample was subjected to the entire procedure at the temperature of liquid nitrogen. The diffraction experiment was carried out using the DN-2 diffractometer at the IBR-2 reactor.

In Fig. 19 we show the sequence of all the neutron-diffraction patterns measured during the process. Their analysis revealed the following. The initial high-pressure phase VIII was preserved up to about 130 K. In the range 130–135 K the peaks corresponding to this crystalline phase completely disappeared over 5 min, and two broad maxima appeared at momentum transfers of 1.72 and 2.09 $Å^{-1}$ with a discontinuity at $Q=1.63$ $Å^{-1}$. These quantities almost exactly coincided with the values 1.63 and 2.10 $Å^{-1}$ observed earlier for amorphous phases of ice and with the value $Q=1.72$ $Å^{-1}$ corresponding to (111) reflection for the cubic phase *Ic*, i.e., a mixture of the two amorphous phases appeared and the first signs of nucleation of the cubic phase were seen. This state was preserved up to 150–160 K, and then the transition to the cubic phase *Ic* occurred. The transition to the hexagonal phase *Ih* occurred at $T\approx230$ K. In addition, it turned out that the transition *Ic*→*Ih* is complicated: first a hexagonal peak (100) appears, i.e., the D_2O molecules are ordered in the base plane of the hexagonal phase, and only then are the planes ordered relative to each other.

Therefore, in this experiment, where the actual measurements of the diffraction spectra were carried out over a period of 6 hours, it was possible to ascertain an entire series of facts: the transition from the VIII phase of ice to the amorphous phase *hda* was observed for the first time, the possibile coexistence of amorphous phases of high and low density was discovered, indicating that the transition *hda*→*lda*, if it occurs, is a first-order transition, and the complex nature of the transition from the cubic to the hexagonal phase was revealed.

Examples of other experiments, including ones with the detection of small-angle neutron scattering, can be found in the review of Ref. 72 and in Ref. 75.

Limiting possibilities for RT experiments at a pulsed neutron source

Following Ref. 76, let us see what limiting values of the time resolution can be expected in the study of irreversible transition processes at a pulsed neutron source and how they are related to the time resolution attained at a stationary reactor.

In the examples of experiments described above the time for measuring a single neutron-diffraction pattern ranged from several seconds to minutes. For the IBR-2 the period of repetition of the power pulses is 0.2 s, i.e., the information was collected during ten or more pulses from the reactor. In principle, when the power of the source or the solid angle of the detector system is increased, a single power pulse is sufficient for collecting the needed statistics. This is actually confirmed by calculations and by the result of a model experiment with a sample of polycrystalline molybdenum (Fig. 20). Thus, a step of 200 ms is the actual value, which is also needed if the characteristic time of the studied process is several seconds.

However, if the situation is reached where one pulse is sufficient for collecting the statistics, it will be possible to

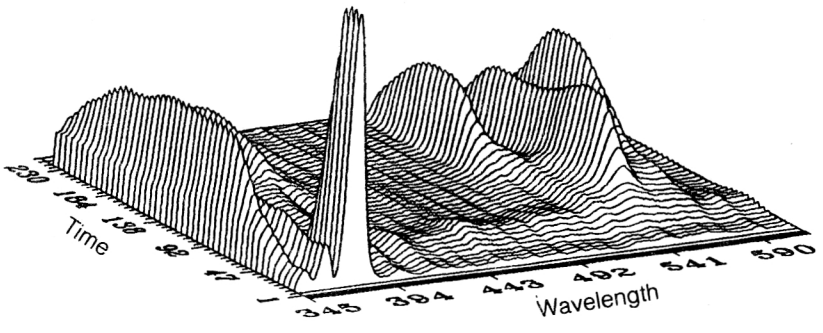

FIG. 19. A sequence of neutron-diffraction patterns measured during the heating of hard ice in the high-pressure phase VIII from 94 to 290 K. The intense peak at the origin of the time scale corresponds to the initial phase VIII. After its decay to the amorphous state, diffraction peaks gradually appear, corresponding to the cubic and hexagonal phases of ice. The heating was done at a rate of ~1 deg/min, and the neutron-diffraction patterns were measured with $t_s=5$ min. The time and wavelength scales are given in conventional units.

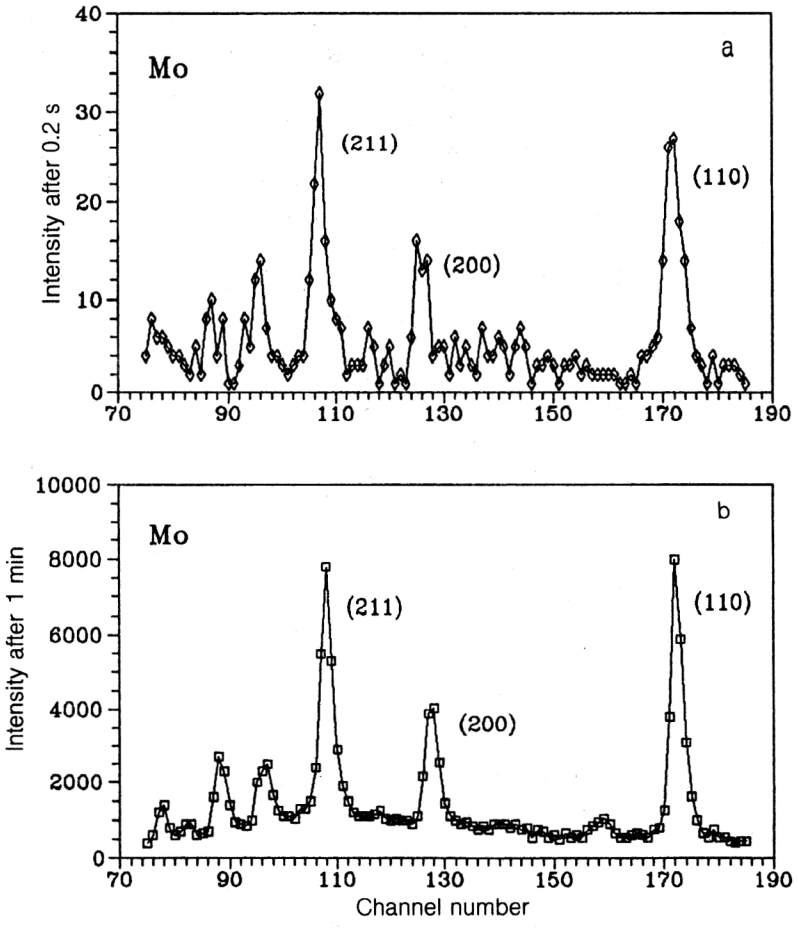

FIG. 20. (a) Neutron-diffraction patterns from a sample of polycrystalline molybdenum of weight 40 g demonstrating the possibility of obtaining the needed statistics from a single pulse of the IBR-2 reactor, $t_s=0.2$ s. (b) For comparison the spectrum measured for 300 pulses is shown ($t_s=1$ min).

make considerably greater progress using a pulsed source by means of the following device. According to the Bragg law, when the scattering angle is changed by $\Delta\theta$ the diffraction peak is shifted in wavelength by $\Delta\lambda=2d\sin\theta\Delta\theta$, which, for example, for the DN-2 diffractometer is equivalent to a time shift of $\Delta t=17.8\Delta\theta$ ms for $d=2$ Å and $2\theta=90°$. That is, several detectors located at scattering angles of 90° with a shift of 3° will record the same diffraction peak with a time shift of 1 ms. In this case the lower limit on t_s is determined by the width of the diffraction peaks (300 μs for DN-2), and the characteristic times of the processes should not greatly exceed 10 ms, because this is precisely the time during which the sample is bombarded with the most intense part of the neutron spectrum.

In principle, a stationary reactor of power 150 MW could ensure the needed conditions for operating with the lower limit $t_s\sim0.1$ s. However, despite the fact that there are plans for 100 and 300 MW reactors, it is unlikely that they will be built in the next few years.

CONCLUSION

In recent years neutron diffraction at pulsed sources has gone through impressive development. The use of pulsed sources has made it possible to overcome the practical limit on the density 10^{15} neutrons/cm^2/s of the neutron flux from the surface of the moderator characteristic of stationary reactors, and also to significantly improve the resolution of neutron diffractometers. The current record characteristics are a flux of $\sim10^{16}$ neutrons/cm^2/s (IBR-2, JINR) and a resolution of 0.0005 (HRPD and HRFD), which have made it possible to reach a qualitatively new level in the solution of diffraction problems—a time resolution of seconds in real-time experiments and *ab initio* determination of the structure in an experiment on polycrystals.

The further development of neutron diffraction using pulsed sources will apparently be achieved mainly by improvement of existing techniques.

Plans for improving the existing sources include, for example, shortening the duration of the fast-neutron pulse (by a factor of 2) at the IBR-2 and increasing the proton current at the target (by a factor of 2–3) at ISIS (Ref. 77). This modernization, which will undoubtedly improve the quality of the experiments, is, however, not fundamental.

There is more promise in the development of TOF diffractometers themselves. For example, the level of luminosity attained is $J\approx10^6$ at the DN-2 diffractometer (IBR-2, JINR), but it is quite realistic to reach $J=(2\text{–}4)\times10^7$ at this source, i.e., an improvement by a factor of 20 to 40 (Ref. 78). This would make it possible to go from test experiments with the recording of the neutron-diffraction pattern from a single pulse of the source to practical studies of irreversible transition processes in a crystal with a time resolution of the order of 1 ms. So far, this resolution has been attained in diffraction experiments only by using synchrotron-radiation sources.

The development of the Fourier method of recording diffraction spectra also holds great promise. At sources of the SNS type high-resolution diffractometers lose a great deal in luminosity because the moderator is optimized in the pulse width and also because of the need to transmit one or several pulses to eliminate overlap of the spectra on the path lengths. Use of the Fourier method would allow a significant improvement in the luminosity due to optimization of the moderator in the neutron yield and shortening of the path length, while keeping the resolution high. Estimates show that even when the transmission factor of the Fourier chopper (~ 0.25) and the correlation background are included, the gain in the luminosity can be ~ 10. Of course, it is necessary to take into account the great technical complexity and expense of installation for an F diffractometer.

Another promising application of the Fourier method might be its use in transmission geometry. As shown in Ref. 79, here there are two important effects: the angular contribution to the resolution function disappears and, consequently, $\Delta d/d$ can be reduced to 0.0003. In addition, by using the procedure of filtering the measured transmission spectrum, it is possible to use the Bragg jumps to determine the values of the structure factors without introducing corrections for the effective neutron spectrum, absorption, and extinction, thereby sharply decreasing the systematic errors.

As far as the construction of new pulsed sources is concerned, a fundamental step forward would be increase of the flux of the thermal-neutron pulse up to 10^{17} neutrons/cm^2/s. Although so far there are only estimates[80] suggesting that this is possible, no discussion of neutron-diffraction problems or diffractometer calculations for such a source have yet appeared.[81]

Of the applications of TOF diffractometers for solving crystallographic and crystallophysics problems discussed here, it is the precision structure analysis of polycrystals which has developed most rapidly and successfully. The structure analysis of single crystals has developed more slowly, but, on the other hand, it is in studies of single crystals that applications of TOF diffractometers appear especially promising. This is true both for structure experiments themselves (analysis of crystals with large elementary cells) and for the so far fairly rare studies with joint analysis of Bragg and diffuse scattering from crystals with partially disordered structure. In the future there will certainly be successful development of TOF diffractometers for neutron diffraction in real time. This topic involves an enormous number of problems closely overlapping with problems in chemistry, biology, the study of materials, and other sciences of both a fundamental and an applied (industrial) nature, and pulsed neutron sources may play the leading role.

[1] R. M. Brugger, Phys. Today **21**, 23 (1968).
[2] Yu. Z. Nozik, R. P. Ozerov, and K. Hennig, *Structure Neutron Diffraction* [in Russian] (Atomizdat, Moscow, 1979], Vol. 1.
[3] H. Fuess, in *Modern Physics in Chemistry*, edited by E. Fluck and V. I. Goldanskiĭ (Academic Press, London, 1979), Vol. 2, p. 1.
[4] Yu. A. Aleksandrov, É. I. Sharapov, and L. Cher, *Diffraction Methods in Neutron Physics* [in Russian] (Énergoizdat, Moscow, 1981).
[5] K. Windsor, *Scattering of Thermal Neutrons from Pulsed Sources* [Russian transl., Énergoatomizdat, 1985].
[6] *Thermal Neutron Scattering*, edited by P. A. Egalstaff (Academic Press, New York, 1965) [Russian transl., Atomizdat, Moscow, 1971].
[7] I. M. Frank, Fiz. Elem. Chastits At. Yadra **2**, 805 (1971) [Sov. J. Part. Nucl. **2**, No. 4, 1 (1972)].
[8] B. Buras, in *Proc. of the Neutron Diffraction Conf.*, RCN-234, Petten, 1975, p. 307.
[9] F. L. Shapiro, *Collected Works* [in Russian] (Nauka, Moscow, 1976), Vol. 2.
[10] V. D. Ananiev, Zh. A. Kozlov, V. I. Luschikov *et al.*, in *Proc. of the Conf. on Neutron Scattering in the Nineties*, IAEA, Vienna, 1985, p. 63.
[11] G. H. Langer and J. M. Carpenter, *ibid.*, p. 17.
[12] D. J. Picton, D. K. Ross, and A. D. Taylor, J. Phys. D **15**, 2369 (1982).
[13] J. D. Jorgensen and F. J. Rotella, J. Appl. Crystallogr. **15**, 27 (1982).
[14] A. M. Balagurov, A. I. Beskrovnyĭ, and N. Popa, Report R3-84-765, JINR, Dubna (1984) [in Russian].
[15] C. R. Hubbard, C. O. Quicksall, and R. A. Jacobson, Acta Crystallogr. A **28**, 236 (1972).
[16] *Neutron Cross Sections*, edited by S. F. Mughabghab, M. Divadeeman, and H. E. Holden (Academic Press, New York, 1981), Vol. 1.
[17] S. Tomiyoshi, M. Yamada, and H. Watanabe, Acta Crystallogr. A **36**, 600 (1980).
[18] N. C. Popa, Acta Crystallogr. A **43**, 304 (1987).
[19] W. H. Zachariasen, Acta Crystallogr. A **23**, 558 (1967).
[20] J. M. Carpenter, Nucl. Instrum. Methods **47**, 179 (1967); A. Holas, Nucleonika **8**, 871 (1968).
[21] W. I. F. David, W. T. A. Harrison, and M. W. Johnson, Report RAL 86-068, Rutherford Appleton Laboratory, Chilton (1986).
[22] P. Hiismaki, V. A. Trunov, O. Antson *et al.*, in *Proc. of the Conf. on Neutron Scattering in the Nineties*, IAEA, Vienna, 1985, p. 453.
[23] P. Hiismaki, H. Poyry, and A. Tiitta, J. Appl. Crystallogr. **21**, 349 (1988).
[24] V. L. Aksenov, O. Antson, A. M. Balagurov *et al.*, Report R3-91-172, JINR, Dubna (1991) [in Russian].
[25] P. Hiismaki, in *Proc. of the Symp. on Neutron Inelastic Scattering*, IAEA, Vienna, 1972, p. 803.
[26] H. M. Rietveld, J. Appl. Crystallogr. **2**, 65 (1969).
[27] A. K. Cheetham and J. C. Taylor, J. Solid State Chem. **21**, 253 (1977).
[28] M. Sakata and M. J. Cooper, J. Appl. Crystallogr. **12**, 554 (1979).
[29] F. Izumi, H. Asano, H. Mutata, and N. Watanabe, J. Appl. Crystallogr. **20**, 411 (1987).
[30] S. Ikeda and J. M. Carpenter, Nucl. Instrum. Methods A **239**, 536 (1985).
[31] V. B. Zlokazov, Nucl. Instrum. Methods **143**, 151 (1977).
[32] R. M. Ibberson and W. I. F. David, in *Proc. of the Sixth School of Neutron Physics*, Alushta, 1990, Report D13,14-91-154, JINR, Dubna (1991), Vol. II, p. 74.
[33] G. E. Jeffrey *et al.*, J. Am. Chem. Soc. **107**, 6227 (1985).
[34] A. K. Cheetham, W. I. F. David, M. M. Eddy *et al.*, Nature **320**, 46 (1986).
[35] A. M. Balagurov, G. M. Mironova, I. S. Lyubutin *et al.*, Superconductivity **3**, 615 (1990).
[36] J. C. Taylor, Aust. J. Phys. **38**, 519 (1985).
[37] P. Day, M. Rosseinsky, K. Prassides *et al.*, J. Phys. C **20**, L429 (1987).
[38] O. Antson, P. Hiismaki, H. O. Poyry *et al.*, Solid State Commun. **64**, 757 (1987).
[39] J. D. Jorgensen, M. A. Beno, D. G. Hinks *et al.*, Phys. Rev. B **36**, 3608 (1987).
[40] G. H. Kwei *et al.*, Phys. Rev. B **39**, 7378 (1989).
[41] N. Niimura, T. Kubota, M. Sato *et al.*, Nucl. Instrum. Methods **173**, 517 (1980).
[42] A. M. Balagurov, V. I. Gordeliy, M. Z. Ishmukhametov *et al.*, Nucl. Instrum. Methods **193**, 617 (1982).
[43] A. M. Balagurov, L. Borca, M. Dlouha *et al.*, Acta Crystallogr. A **35**, 131 (1979).
[44] M. R. Anderson, G. T. Jenkin, and J. M. White, Acta Crystallogr. B **33**, 3933 (1977).
[45] A. I. Beskrovnyj, M. Dlouha, Z. Jirak *et al.*, Physica C **166**, 79 (1990).
[46] A. M. Balagurov, F. Prokert, and B. N. Savenko, Phys. Status Solidi A **103**, 131 (1987).
[47] B. N. Savenko, D. Sangaa, and F. Prokert, Ferroelectrics **107**, 207 (1990).
[48] B. P. Schoenborn, Nature **224**, 143 (1969).

[49] D. Bally, A. M. Balagurov, V. Chirtoc *et al.*, Report IFA, FN-48-1975, Bucharest (1975).
[50] S. Ramaseshan, Curr. Sci. **35**, 87 (1966).
[51] A. K. Singh and S. Ramaseshan, Acta Crystallogr. B **24**, 35 (1968).
[52] A. M. Balagurov, V. E. Novozhilov, Yu. M. Ostanevich, and V. D. Shibaev, Report R14-12840, JINR, Dubna (1979) [in Russian].
[53] A. M. Balagurov, I. P. Barabash, and V. D. Shibaev, Prib. Tekh. Eksp. **2**, 79 (1977) [Instrum. Exp. Tech (USSR)].
[54] A. M. Balagurov, I. D. Dutt, Z. Gheorghiu, *et al.*, Phys. Status Solidi A **51**, 367 (1979).
[55] G. S. Parry, Acta Crystallogr. **15**, 596 (1962).
[56] A. M. Balagurov, I. D. Dutt, B. N. Savenko, and L. A. Shuvalov, Fiz. Tverd. Tela (Leningrad) **22**, 2735 (1980) [Sov. Phys. Solid State **22**, 1595 (1980)].
[57] L. A. Shuvalov, A. M. Balagurov, B. N. Savenko, and I. D. Dutt, Ferroelectrics **29**, 213 (1980).
[58] A. M. Balagurov, A. I. Beskrovnyĭ, I. D. Dutt *et al.*, Report 14-84-69, JINR, Dubna (1984) [in Russian].
[59] A. M. Balagurov, B. Mroz, N. C. Popa, and B. N. Savenko, Phys. Status Solidi A **96**, 25 (1986).
[60] A. M. Balagurov, S. B. Bakhrushev, A. A. Neberezhnov *et al.*, Report R14-90-423, JINR, Dubna (1990) [in Russian].
[61] A. M. Balagurov, V. I. Gordeliy, and L. S. Yaguzhinskiĭ, Biofizika **31**, 31 (1986).
[62] A. M. Balagurov, A. I. Beskrovnyĭ, and N. Popa, Report R3-87-531, JINR, Dubna (1987) [in Russian].
[63] I. A. Vasilenko, L. A. Tonkonog, A. M. Balagurov *et al.*, Biol. Membrany **5**, 428 (1988) [in Russian].
[64] A. M. Balagurov, V. I. Gordeliy, and G. Kloze, Report R14-87-804, JINR, Dubna (1987) [in Russian].
[65] N. Niimura and M. Muto, Nucl. Instrum. Methods **126**, 87 (1975).
[66] D. Georgiev, V. V. Nitts, and A. A. Yakovlev, Report R14-89-758, JINR, Dubna (1989) [in Russian].
[67] J. Pannetier, in *Proc. of the NATO-ASI Institute*, edited by M. A. Carrondo and G. A. Jeffrey (Reidel, Dordrecht, 1988), p. 313.
[68] I. V. Naumov, V. P. Glazkov, A. V. Irodova *et al.*, Report IAÉ, 4204/9, Moscow (1985) [in Russian].
[69] A. M. Balagurov and G. M. Mironova, Superconductivity **3**, 545 (1990).
[70] A. M. Balagurov and G. M. Mironova, in *Proc. of the Sixth School of Neutron Physics*, Alushta, 1990, Report D13,14-91-154, JINR, Dubna (1991), Vol. II, p. 16.
[71] A. M. Balagurov, V. I. Gordeliy, and L. S. Yaguzhinskiĭ, Biofizika **31**, 1004 (1986).
[72] A. M. Balagurov and G. M. Mironova, Kristallografiya **36**, 314 (1991) [Sov. Phys. Crystallogr. **36**, 162 (1991)].
[73] A. M. Balagurov, O. I. Barkalov, A. I. Kolesnikov *et al.*, Pis'ma Zh. Eksp. Teor. Fiz. **53**, 30 (1991) [JETP Lett. **53**, 30 (1991)].
[74] D. D. Klug, Y. P. Handa, J. S. Tse, and E. J. Whalley, J. Chem. Phys. **90**, 2390 (1989).
[75] A. M. Balagurov, G. M. Mironova, and V. G. Simkin, in *Progress in High-T_c Superconductivity*, edited by V. L. Aksenov, N. N. Bogolyubov, and N. M. Plakida (World Scientific, Singapore, 1989), Vol. 21, p. 263.
[76] G. M. Mironova, Report R13-898-326, JINR, Dubna (1988) [in Russian].
[77] *Proc. of the Conf. on Neutron Scattering in the Nineties*, IAEA, Vienna (1985).
[78] A. M. Balagurov, Physica B **174**, 542 (1991).
[79] P. Hiismaki, J. Appl. Crystallogr. **22**, 79 (1989).
[80] Yu. Ya. Stavisskiĭ, in *Proc. of the Fourth School on Neutron Physics*, JINR, Report D3,4-82-704, JINR, Dubna, 1982, p. 342 [in Russian].
[81] J. D. Jorgensen, D. E. Cox, A. W. Hewat, and W. B. Yelon, in *Proc. of the Shelter Island Workshop on Scientific Opportunities With Advanced Facilities for Neutron Scattering*, 1984, p. 45.

Translated by Patricia A. Millard